



Cerebellar compartmentation of prion pathogenesis

Audrey Ragagnin, Juliette Ezpeleta, Aurélie Guillemain, François Boudet-Devaud, Anne-Marie Haeberlé, Valérie Demais, Catherine Vidal, Stanislas Demuth, Vincent Béringue, Odile Kellermann, et al.

► To cite this version:

Audrey Ragagnin, Juliette Ezpeleta, Aurélie Guillemain, François Boudet-Devaud, Anne-Marie Haeberlé, et al.. Cerebellar compartmentation of prion pathogenesis. Brain Pathology, 2018, 28 (2), pp.240-263. 10.1111/bpa.12503 . hal-02363123

HAL Id: hal-02363123

<https://hal.science/hal-02363123>


Submitted on 10 Nov 2021

HAL is a multi-disciplinary open access archive for the deposit and dissemination of scientific research documents, whether they are published or not. The documents may come from teaching and research institutions in France or abroad, or from public or private research centers.

L'archive ouverte pluridisciplinaire **HAL**, est destinée au dépôt et à la diffusion de documents scientifiques de niveau recherche, publiés ou non, émanant des établissements d'enseignement et de recherche français ou étrangers, des laboratoires publics ou privés.

RESEARCH ARTICLE

Cerebellar compartmentation of prion pathogenesis

Audrey Ragagnin¹, Juliette Ezpeleta², Aurélie Guillemain¹, François Boudet-Devaud², Anne-Marie Haeberlé¹, Valérie Demais³, Catherine Vidal⁴, Stanislas Demuth¹, Vincent Béringue⁵, Odile Kellermann², Benoit Schneider², Nancy J. Grant¹, Yannick Bailly ¹

¹ Cytologie et Cytopathologie Neuronales, Institut des Neurosciences Cellulaires & Intégratives, CNRS UPR 3212, Strasbourg, France.

² INSERM UMR-S1124, Cellules Souches, Signalisation et Prions, Université Paris Descartes, Paris, France.

³ Plateforme Imagerie In Vitro, CNRS UPS-3156, Université de Strasbourg, Strasbourg, France.

⁴ Institut Pasteur, Paris, France.

⁵ VIM, INRA, Université Paris-Saclay, Jouy-en-Josas, France.

Keywords

cerebellar compartmentation, inflammation, prion, Purkinje cell, zebrin.

Corresponding author:

Yannick Bailly, PhD, Cytologie et Cytopathologie Neuronales, Institut des Neurosciences Cellulaires & Intégratives, CNRS UPR 3212, Strasbourg, France (E-mail: byan@inci-cnrs.unistra.fr)

Received 29 November 2016

Accepted 1 March 2017

Published Online Article Accepted

7 March 2017

doi:10.1111/bpa.12503

Abstract

In prion diseases, the brain lesion profile is influenced by the prion “strain” properties, the invasion route to the brain, and still unknown host cell-specific parameters. To gain insight into those endogenous factors, we analyzed the histopathological alterations induced by distinct prion strains in the mouse cerebellum. We show that 22L and ME7 scrapie prion proteins (PrP^{22L}, PrP^{ME7}), but not bovine spongiform encephalopathy PrP^{6PB1}, accumulate in a reproducible parasagittal banding pattern in the cerebellar cortex of infected mice. Such banding pattern of PrP^{22L} aggregation did not depend on the neuroinvasion route, but coincided with the parasagittal compartmentation of the cerebellum mostly defined by the expression of zebrins, such as aldolase C and the excitatory amino acid transporter 4, in Purkinje cells. We provide evidence that Purkinje cells display a differential, subtype-specific vulnerability to 22L prions with zebrin-expressing Purkinje cells being more resistant to prion toxicity, while in stripes where PrP^{22L} accumulated most zebrin-deficient Purkinje cells are lost and spongiosis accentuated. In addition, in PrP^{22L} stripes, enhanced reactive astrocyte processes associated with microglia activation support interdependent events between the topographic pattern of Purkinje cell death, reactive gliosis and PrP^{22L} accumulation. Finally, we find that in preclinically-ill mice prion infection promotes at the membrane of astrocytes enveloping Purkinje cell excitatory synapses, upregulation of tumor necrosis factor- α receptor type 1 (TNFR1), a key mediator of the neuroinflammation process. These overall data show that Purkinje cell sensitivity to prion insult is locally restricted by the parasagittal compartmentation of the cerebellum, and that perisynaptic astrocytes may contribute to prion pathogenesis through prion-induced TNFR1 upregulation.

INTRODUCTION

Conversion of the host-encoded cellular prion protein PrP^C to abnormal insoluble isoforms PrP^{TSE} in the central nervous system (CNS) (18) is at the root of transmissible spongiform encephalopathies (TSEs), a group of fatal neurodegenerative disorders commonly named prion diseases, that affect both human and animals (1, 97, 98). The histopathological signature of TSEs notably relies on the aggregation of PrP^{TSE}, vacuolation of the brain tissue, astrogliosis and neuronal loss. Among TSEs, scrapie is a natural ovine prion disease widely studied in mouse models with the help of murine-adapted prion strains (22L, ME7) that, akin to natural prion strains, differ in the rate of disease progression (ie, duration of the incubation period), as well as the extent and regional pattern of brain histopathology (20, 65). For instance, the characteristic of a prion strain mostly relies on specific biochemical properties related

to PrP^{TSE} misfolding. The variable susceptibility of neuronal types to prion infection also emerges as another critical prion strain parameter that underlies the complex mechanisms of prion pathogenesis (32, 77, 118) and PrP^{TSE} progression along defined anatomical routes (11). The cellular and molecular mechanisms involved in the targeting of PrP^{TSE} to specific neuronal populations (43, 56, 116) and the neuron-to-neuron spreading of prions in the CNS remain however elusive (117).

In several prion diseases, the cerebellum emerges as a preferential target of prions in scrapie (42, 45, 68, 79, 128) or in Creutzfeldt-Jakob disease (CJD) cases (6, 12, 21, 23, 37, 57, 92, 109, 132). Quantitative studies performed in post-mortem brains from individuals with sporadic (4), familial (70) and variant CJD (vCJD) (6) revealed topographic patterns of pathological alterations along the cerebellar folia, suggesting that prion pathology spreads

to the cerebellum via anatomically connected pathways (10, 17, 126). Of note, the cerebellar circuits are exquisitely patterned and a cerebellar topographical map of genetically determined zones that control sensory-motor behavior is defined, at least in part, by the expression patterns of zebrins (Z) in Purkinje cells (PCs) (3, 101, 134). Some subsets of PCs expressing zebrins alternate with subsets of zebrin-free PCs, thus forming complementary stripes of biochemically distinct PCs (3). The most comprehensively studied zonal marker is zebrin II (15), also known as aldolase C (ZII/AldC). The expression of ZII/AldC by itself is however not sufficient to recapitulate the full complexity of the cerebellar cortex because of the presence of many other PC subtypes (7, 46, 82). As concerns prion infection, the 22L scrapie strain induces significant PC loss (29) and both PrP^{22L} and PrP^{ME7} prion strains accumulate in the mouse cerebellar cortex according to a transversal banding pattern reminiscent of the cerebellar compartmentation (19, 66, 95). This suggests that the impacts of scrapie prion on cerebellar cell populations may be modulated by some parameters different from one compartment to the other.

In this study, we mainly exploit transgenic mice expressing GFP in EAAT4 PC subtypes (ZII/AldC-expressing PCs) to investigate whether prion infection follows the major pattern of cerebellar compartmentation. Qualitative and quantitative histopathological analyses of the cerebellar cortex reveal that PrP^{22L} accumulation, spongiosis, PC neurodegeneration and gliosis induced by scrapie prions are restricted by this major compartmentation pattern of the cerebellum. This indicates that a yet-to-be identified, patterned local factor modulates scrapie prion pathogenesis in the cerebellar cortex.

MATERIALS AND METHODS

Ethics statements

This study was carried out in strict accordance with the national and international laws for laboratory animal welfare and experimentation (EEC Council Directive 2010/63/EU, September 2010) and was approved by the Comité d'Ethique en Expérimentation Animale de Strasbourg CEEA35 (ref. AL/01/01/01/13) and the INRA Ethics Committee (COMETHEA, permit number 12/034).

Infection of mice

Adult (3-month old) C57Bl/6J mice (wild type (WT), $n = 37$) and C57Bl/6J EAAT4-eGFP transgenic mice ($n = 18$, gift from Dr J. Rothstein (52)), were used. For scrapie infection, mice were anaesthetized with ketamine (80 mg/kg) and xylazine (5 mg/kg) and inoculated by either an intracerebellar (i.cb. right cerebellum) or intracerebral (i.c., right parieto-temporal cortex) injection (2 μ l of a 10% or 20 μ l of a 1% mouse-adapted, 22L scrapie brain homogenate obtained from symptomatic scrapie-infected mice diluted in 0.9% NaCl (122)). Alternatively, mice received 200 μ l of the 1% 22L brain homogenate (WT, $n = 6$; EAAT4-eGFP, $n = 3$) via an intraperitoneal (i.p.) injection. For comparison, WT mice were inoculated i.c. (in the frontal hemisphere) with 20 μ l of a 10% ME7 brain homogenate ($n = 10$) (69) or with 20 μ l of a 1% 6PB1 brain homogenate obtained from symptomatic mice infected with the 6PB1 strain of bovine spongiform encephalopathy (BSE; $n = 3$), as previously described (76). Although contrarily to ME7 and BSE which have been directly isolated from animal sources, the 22L

scrapie strain can be considered as an essentially laboratory-derived strain associated only indirectly with known TSEs, 22L was used in this study because it exhibits a strong cerebellotropism after i.c. and i.p. inoculation and has been widely used in prion research bringing important insights into prion pathogenesis (44, 67, 68, 95, 99, 129). As controls, mock-infected mice were similarly inoculated with brain homogenate from healthy mice. The incubation period was determined as the interval between the injection and a clinical end-point defined by the appearance of unequivocal clinical signs of prion disease (motor impairment, weakening, wasting) (20, 68, 99). The mice were weighed and examined weekly during the preclinical period and daily during the clinical period. The cerebella from i.cb. 22L-infected mice were examined at both preclinical and clinical stages (67), whereas the cerebella from i.c. and i.p. 22L-, ME7- and 6PB1-infected WT and EAAT4-eGFP mice were analyzed at clinical stages of the disease.

Fixation and microtomy

Under ketamine (125 mg/kg) and xylazine (17 mg/kg) anesthesia WT and EAAT4-eGFP mice were perfused with 4% paraformaldehyde (PFA) in 0.1 M phosphate buffer (PB, pH 7.3) and the cerebellum was removed and further fixed for at least 24 h at 4°C. Alternatively, WT mice were decapitated and the cerebellum immersed in Carnoy's fixative for 12 h and then in butanol for at least 3 days. PFA- and Carnoy-fixed cerebella were then dehydrated before paraffin embedding (24, 75). For cryostat sections, the cerebella of EAAT4-eGFP and WT mice were cryoprotected in 30% sucrose in 0.1M PB and then frozen in isopentane (-80°C).

Transverse paraffin and cryostat sections (15 μ m) were cut at the anterior (-5.40 to -6.12), median (-6.24 to -6.96) and posterior (-7.08 to -7.92) levels of the cerebellum of all mice (93). On transverse cerebellar sections of the EAAT4-eGFP mice, the Z+ and Z- PC subsets were clearly distinguishable because only the Z+ PCs displayed green eGFP fluorescence. The compartmentation of EAAT4-eGFP in cryostat and deparaffinized cerebellar sections was photographed (ProgRes CFcool Jenoptik camera on a Zeiss AxioImager microscope) before histological and immunohistochemical staining of sections.

PrP^{22L}, PrP^{ME7} and PrP^{6PB1} immunohistochemistry

Immunoreactive PK-resistant prion protein is globally defined as PrP^{TSE} and specifically as PrP^{22L}, PrP^{ME7} and PrP^{6PB1} in brain tissue inoculated respectively, with mouse-adapted 22L, ME7 and 6PB1 mouse brain homogenates. PrP^{TSE} was revealed in cryostat and deparaffinized cerebellar sections using a classical protocol (121). Sections were incubated in proteinase K (Eurobio, Courtaboeuf, France) diluted 1/5000 in phosphate buffered saline (PBS) containing 0.25% Triton X-100 (PBST) for 10 min at 37°C and subsequently denatured in 3.4 M guanidinium thiocyanate in PBST for 15 min. After rinsing in PBST, endogenous peroxidases were inactivated using either Peroxidase Block (EnVision, Dako, Glostrup, Denmark) or 2% H₂O₂ (in methanol) before blocking in normal goat serum (3% NGS in PBST). Sections were then incubated with a mouse anti-prion protein antibody (SAF32 SPI-Bio/CEA, Fontenay-aux-Roses, France; diluted 1 μ g/ml in PBST containing 0.5% NGS) overnight at 4°C. PrP^{TSE} immunoreactivity was revealed with secondary antibodies coupled to either Alexa 546 (1/200, Molecular

Probes, Eugene, USA) or biotin (diluted 1/200 in PBST) and processed according to the manufacturer's instructions (Immunoperoxidase Envision kit, Dako, Glostrup, Denmark or Elite kit Vector). Immunofluorescent sections were mounted in Mowiol (Calbiochem, Merck-Millipore, Molsheim, France) and the immunoperoxidase sections were mounted in Eukitt (Polylabo, Strasbourg, France).

PrP^{22L} and PrP^{ME7} immunoperoxidase for transmission electron microscopy (TEM)

Floating transverse cryostat sections (50 μ m-thick) were post-fixed in 0.1% glutaraldehyde in 0.1M PB before processing for PrP^{TSE} immunoperoxidase labeling, as described above. Sections were then post-fixed in 1% glutaraldehyde in PB and 0.5% osmium tetroxide in 0.1M PB before dehydrating and embedding in Araldite. Ultrathin sections were photographed with a transmission electron microscope (Hitachi 7500) equipped with a digital camera (AMT Hamamatsu, Japan).

Masson's trichrome and cerebellar lesion profiles

One anterior, one median and one posterior section of the cerebellum from each mouse ($n = 8$ i.p., 5 i.c., 22 i.cb.) was stained with Masson's trichrome (48). To determine the lesion profile, the average degree of vacuolation was scored on a scale ranging from 0 (no vacuoles) to 5 (confluent vacuoles throughout the defined brain region) in the cerebellar cortex, white matter and deep nuclei, as previously described (44, 67).

In 3 clinically ill EAAT4-eGFP mice infected with 22L i.c., the vacuolation score was determined in both intensely and weakly PrP^{22L} immunoperoxidase-stained stripes of the cerebellar cortex. Here, the vacuole density was estimated by directly counting the vacuoles in PrP^{22L} stained sections using differential interference contrast (DIC) optics.

Immunohistochemistry for cell type-specific markers and PrP^{22L}

Before staining for PrP^{22L} or PrP^{ME7}, sections were immunostained for one of the following cell markers: PC markers, calcium binding protein (CaBP mouse 1/100, Sigma C9848, Saint-Louis, USA) and aldolase C (rabbit 1/50, gift from Pr I. Sugihara, Tokyo, Japan); the astrocyte marker glial fibrillary acidic protein (GFAP mouse 1/300, Sigma G3893); the microglial cell marker ionized calcium binding adaptor molecule 1 (Iba1 rabbit 1/250, Wako, Richmond, USA); neuronal markers, neuron-specific nuclear protein (NeuN mouse 1/1000, Millipore, Temecula, USA) and vesicular glutamate transporter 1 (vGLUT1 guinea pig 1/1000, Synaptic Systems, Göttingen, Germany). Immunohistofluorescence was performed using appropriate secondary antibodies (1/500) coupled to Alexa 546 (Molecular Probes), Alexa 555 (Life Technology, Thermo Fisher Scientific, Illkirch-Graffenstaden, France) or Cy3 (Jackson ImmunoResearch, West Grove, USA). After photographing, sections were processed for immunoperoxidase detection of PrP^{22L} as described above.

Immunohistochemistry for TNFR1 and PrP^{22L}

Either immunofluorescence or immunoperoxidase staining (on adjacent sections) was used to reveal tumor necrosis factor- α

receptor 1 (TNFR1) in cryostat and deparaffinized cerebellar sections. In PFA-fixed sections, antigen retrieval was achieved as follows. Briefly, sections were immersed in 10 mM citrate buffer, pH 6 at 100°C for 15 min, before blocking in 3% NGS in PBS, and then incubated overnight at 4°C with rabbit polyclonal anti-TNFR1 antibodies (diluted 1/50 in PBS with 0.3% NGS; MBL International). For immunofluorescence, a secondary goat anti-rabbit antibody conjugated to Alexa 488 (diluted 1/200, Molecular Probes) was used. Sections were examined and photographed with an epifluorescence microscope before being processed for PrP^{22L} immunoperoxidase staining as described above.

Immunohistochemistry for TNFR1 and cell-type specific markers

Following TNFR1 immunofluorescence, sections were processed for immunofluorescent labeling of CaBP, aldolase C, the marker of the parallel fiber terminals (vGLUT1), and the astrocyte markers GFAP and EAAT1/GLAST (1/300, Abcam ab49643, Cambridge, UK) as described above. In some cases, PrP^{22L} immunoperoxidase labeling was performed either on the same section or an adjacent section. Alternatively, Carnoy-fixed cerebellar sections (which did not need TNFR1 antigen retrieval treatment) were processed for TNFR1 immunoperoxidase and immunofluorescent labeling of CaBP, GFAP or aldolase C on adjacent sections before PrP^{22L} immunoperoxidase staining. Sections were examined and photographed with a confocal microscope (63 \times objective, $na = 1.4$, Leica SP5, Nanterre, France).

TNFR1 immunoperoxidase labeling for TEM

After processing for antigen retrieval as described above, floating transverse cryostat sections (50 μ m-thick) were incubated in blocking solution (0.5% NGS, 0.1% cold water fish skin gelatin and 0.5% bovine serum albumin in PBS) before incubating with anti-TNFR1 primary antibodies as described above. Immunoperoxidase labeling, post-fixation and processing for TEM was carried out as described above for PrP^{TSE} experiments.

Quantitative analysis of PCs

One paraffin (22L i.p. and i.cb.) or cryostat (22L i.c. and i.p.) section was selected at the anterior, median and posterior levels of the cerebellum from sham mice ($n = 6$) and 22L-infected wild-type and EAAT4-eGFP mice (i.p. $n = 7$; i.c. $n = 4$; i.cb. $n = 8$) and PCs were stained for CaBP (immunoperoxidase or immunofluorescence) or aldolase C (immunofluorescence) as described above.

The layer of PC bodies occupies the interface between the molecular layer (ML) and the internal granular layer (IGL). Thus, the linear density of PCs is "the number of PCs per unit of PC monolayer length". To determine the linear density of PCs, the length of this interface was measured and the number of CaBP-labeled PC somata present was counted throughout the vermis and the hemispheres of each section using ImageJ. Similarly, the linear densities of EAAT4- or aldolase C-expressing and non-expressing PCs were determined in merged images of EAAT4-eGFP or aldolase C-Alexa 488 and CaBP labeling. Finally, the linear densities of PCs in PrP^{22L}+ and PrP^{22L}- stripes were determined in merged images of PrP^{22L} and CaBP labeling using the same method.

Quantitative analysis of granule cells and interneurons

One paraffin section was selected at the anterior, median and posterior levels of the cerebellum of sham mice ($n = 5$) and 22L-infected wild-type mice (i.p. $n = 5$; i.c. $n = 3$; i.cb. $n = 8$) and the neuronal nuclei immunoperoxidase stained for NeuN, as described above. In addition, cryostat sections were similarly selected from the cerebellum of sham mice ($n = 3$) and 22L-infected EAAT4-eGFP mice ($n = 3$) and immunofluorescence labeled for NeuN. In the ML, most of the immunostained nuclei corresponded to basket and stellate interneurons, whereas in the IGL, the immunostained nuclei belonged almost exclusively to granule cells (the large nuclei of the Golgi interneurons reacted weakly and were excluded from the analysis). The density of granule cells in the IGL was calculated as the ratio of the IGL area in each section and the mean granule cell nucleus area measured from 50 randomly selected NeuN-immunoreactive cells. Similarly, the granule cell density was compared between stripes with intense and weak PrP^{22L} immunoreactivity throughout the cerebellar sections. Finally, the mean densities of basket and stellate interneurons in the ML were determined in the same way.

Statistics

Data are given as mean values \pm standard error of the mean (SEM). Statistical comparisons between group means were performed using SigmaPlot. The extent of spongiosis, the mean linear densities of PCs in addition to the densities of microglial cells and granule cell nuclei and interneuron nuclei, were compared between anterior, median and posterior cerebellar levels, between vermis and hemispheres, and between total cerebellum in sham and 22L i.c., i.cb. and i.p.-infected groups using one- or two- way (inoculation route, cerebellar compartments) ANOVA followed by *post hoc* Tukey tests for multiple comparisons when justified. This test was also used to compare cell densities in strongly and weakly stained PrP^{22L} stripes in infected cerebella. When the assumptions of ANOVA were not met, groups were compared by using a Kruskal–Wallis test followed by a *post hoc* Dunn's test for multiple comparisons as indicated. The significance threshold was set at $P = 0.05$.

Imaging

Final adjustment of contrast and brightness was performed using Photoshop 7.0. The original PrP immunoperoxidase images were converted into black and white, inverted and finally converted to red or green. The yielded image was then merged with the corresponding immunofluorescent marker images.

RESULTS

PrP^{22L} and PrP^{ME7} but not PrP^{6PB1} accumulate in parasagittal stripes in the mouse cerebellar cortex

To analyze prion protein accumulation in the cerebellum in connection with the prion strain and route of invasion, C57Bl6/7J mice were inoculated by i.c., i.cb. or i.p. with the mouse-adapted 22L (PrP^{22L}) or ME7 (PrP^{ME7}) scrapie strains, or the 6PB1 (PrP^{6PB1}) bovine spongiform encephalopathy (BSE) strain.

We first probed signs of cerebellar dysfunction in prion-infected mice. Mice inoculated by i.c. and i.cb. with PrP^{22L} exhibited the first clinical signs of infection, that is, gait disturbance and ataxia, as early as 131 dpi and 134 dpi, respectively. Additional symptoms, such as arched back, tail rigidity, ruffled fur, keratitis and hind limb paresis, gradually developed up to the pre-terminal stage at 152 dpi, at which time animals were sacrificed. As expected, mice inoculated i.p. with 22L developed initial symptoms much later at 184 ± 2.6 dpi, and the terminal stage occurred at 235 ± 4 dpi. Mice inoculated i.c. with PrP^{ME7} developed similar clinical signs at 147 dpi. Irrespective of the scrapie prion strain and the route of inoculation, such clinical signs argue for cerebellar functional alterations induced by prion infection. In the case of the 6PB1 BSE strain, mice inoculated i.c. first showed impaired motor coordination at 155 ± 1.5 dpi ($n = 3$) (121), and the additional symptoms developed up to the terminal stage at 188 ± 1.3 dpi.

In the cerebellum of the 22L i.cb.-infected mice, PrP^{22L} was detected as early as 92 dpi during the preclinical period. At 92 dpi, PrP^{22L} surrounded neurons in the deep cerebellar nuclei (Figure 1A). In the cerebellar cortex, scattered spots and plaques of PrP^{22L} first appeared in the internal granular layer (IGL) and to a lesser extent in the molecular and Purkinje cell (PC) layers (Figure 1B). PrP^{22L} formed tiny granular deposits in the molecular layer, and was concentrated at the periphery of PCs between granule cells. Most of the PrP^{22L} deposits in the molecular layer (ML) were topographically coincident with PrP^{22L} accumulation in the subjacent PC and internal granular layers (Figure 1C,G). These observations suggest that the neuroinvasion of the cerebellar cortex by 22L prions progresses from the IGL to the ML or PrP^{22L} accumulates faster in the IGL. Vertical palisades of PrP^{22L} formed clear-cut stripes in the cortex of the crus I folium in the hemispheres (Figure 1C). Elsewhere in the cerebellum, PrP^{22L} deposits in the IGL were observed in lobules III, IV–V, VI and IX of the vermis and in all folia of the hemispheres (Figure 1B–D,G,H). At 107 dpi of the pre-clinical period, PrP^{22L} deposits increased throughout the deep cerebellar nuclei (Figure 1E,F) and formed patches in the IGL of all lobules in the vermis and the hemispheres of the cerebellar cortex. Whereas PrP^{22L} deposits appeared more or less diffusely distributed in the IGL, they formed vertical palisades in the ML of almost all lobules of the vermis (II–X), and in the copula, paramedian and crus folia of the hemispheres. In addition, clear-cut, compact stripes were observed in the posterior lobules of the vermis and all folia of the hemispheres (Figure 1D–H).

During the clinical period, PrP^{22L} invaded the deep cerebellar nuclei (Figure 2A), as well as the cortex of all lobules (Figure 2B–D,E), but was never detected in the cerebellar white matter. Of note, the PrP^{22L} topography in the cerebellar cortex of clinically ill mice inoculated i.cb. (134–156 dpi, Figure 2A–E) was similar in the cerebellar cortex of clinically ill mice inoculated i.c. (132–153 dpi, data not shown) or i.p. (165–235 dpi, data not shown), indicating that the invasion route does not impact on PrP^{22L} tropism in the cerebellum.

Interestingly, PrP^{22L} accumulated vertically, delineating clear-cut, parasagittal stripes of staining in all lobules of the vermis and the hemispheres (Table 1). In these stripes, PrP^{22L} was present in the ML, as well as in the subjacent IGL, whereas the surrounding cortex displayed only weak, if any, PrP^{22L} staining. The full pattern was composed of a median PrP^{22L} stripe flanked by at least 7 parasagittal PrP^{22L} stripes from the vermis to the hemispheres (Figure 2C–E). Notably, a characteristic banding pattern already appeared

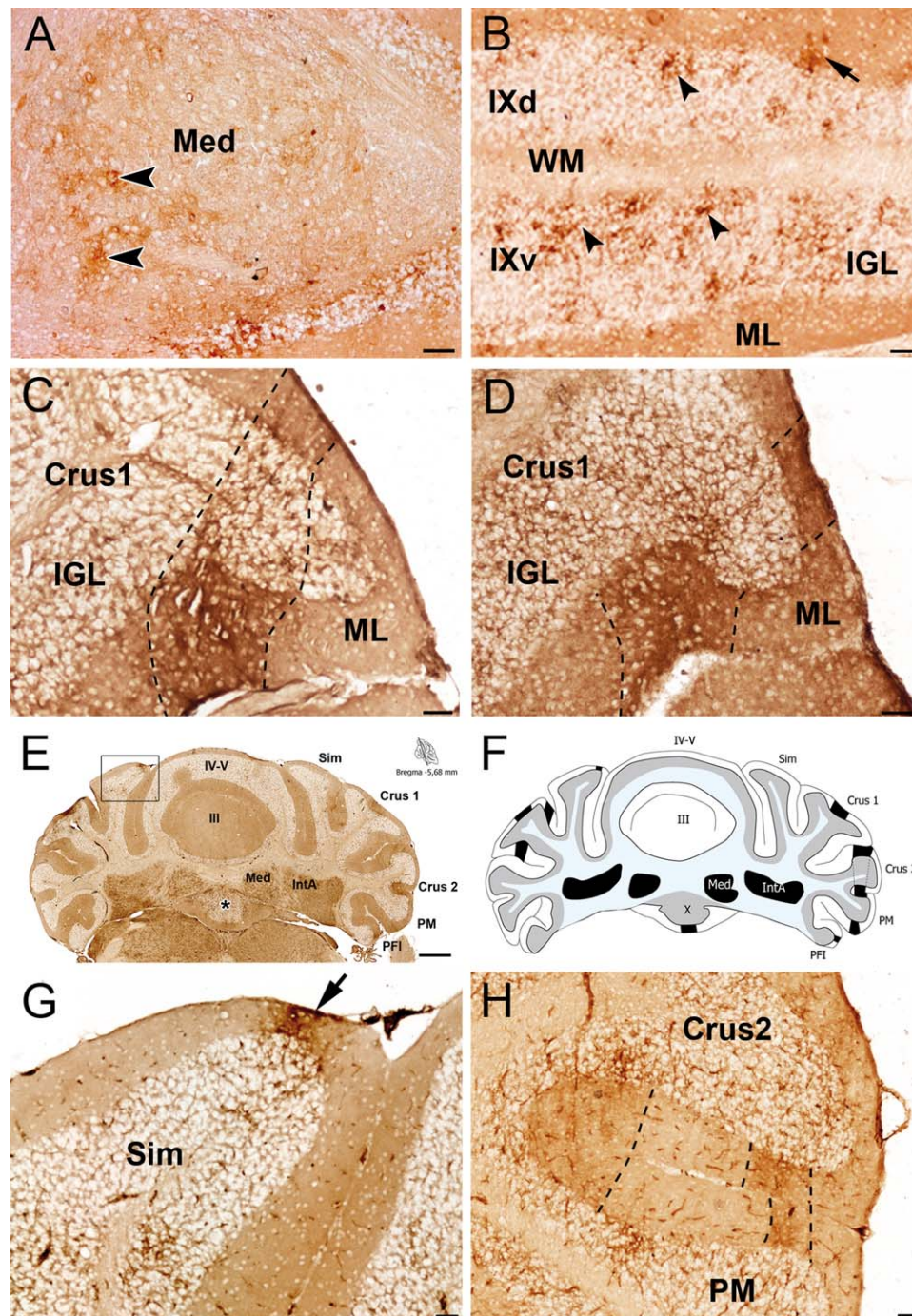


Figure 1. Immunoperoxidase staining of PrP^{22L} in the cerebellum of i.c.b. inoculated mice during preclinical (92–107 dpi) period. **A.** PrP^{22L} deposits (arrowheads) around the neurons in the medial (fastigial) cerebellar nucleus (Med). **B.** Diffuse PrP^{22L} deposits in IGL (arrowheads) and ML (arrow) of dorsal (IXd) and ventral (IXv) sides of lobule IX. WM, white matter. **C,D.** A stripe of PrP^{22L} (between dotted lines) in the cortex of Crus1 at early (C, 92 dpi) and late (D, 107 dpi) preclinical stages of the disease. PrP^{22L} forms vertical palisades in the molecular layer (ML) and accumulates between granule cells in the subjacent internal granular layer (IGL). **E,F.** Banding pattern of PrP^{22L} aggregates in the anterior cerebellum (bregma—5.68 mm). E. PrP^{22L} is apparent throughout the

median (Med) and anterior interposed (IntA) deep nuclei, whereas several stripes of PrP^{22L} have already formed in the cortex of the simple (Sim), crus1, crus2, paramedian (PM) and paraflocculus (PFI) of the hemispheres. PrP^{22L} deposits are scarce in the vermis except in the Xth lobule where a median PrP^{22L} stripe and diffuse PrP^{22L} accumulation throughout IGL (*) are observed in the cortex. Bar = 500 μ m. F. Schematic mapping of PrP^{22L} immunoperoxidase staining (black areas) shown in E. **G.** Magnification of the inset in E. PrP^{22L} stripe (arrow) forming at the apex of Sim. **H.** The crus 2 (Crus2) and paramedian lobule (PM) display a characteristic pattern of PrP^{22L} stripes (between dotted lines) which is reproduced at the clinical stages in all mice. Bar = 50 μ m.

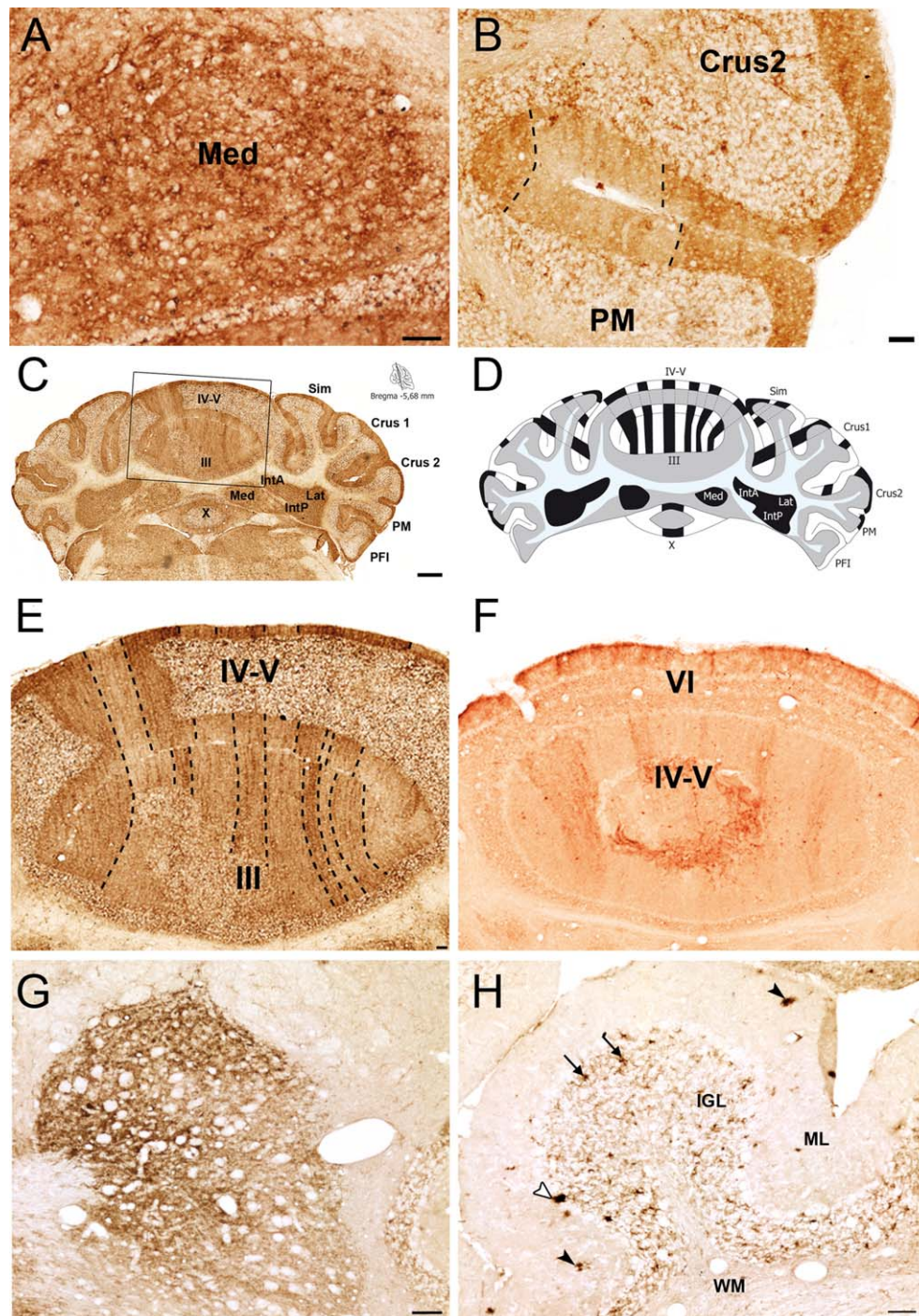


Figure 2. Immunoperoxidase staining of PrP^{22L}, PrP^{ME7} and PrP^{6PB1} in the mouse cerebellum at clinical stages (134–139 dpi) of the diseases. **A–E.** i.c.b. inoculated mice. **A.** PrP^{22L} deposits around the neurons have invaded the medial (fastigial) cerebellar nucleus (Med) at the clinical stage of the disease. **B–E.** Banding pattern of PrP^{22L} aggregates in the anterior (**C–E**) and median (**B**, bregma –6.64 mm) cerebellum. **B.** Same legend as Figure 1H. **C.** At the clinical stage of the disease, PrP^{22L} stripes are clearly visible in the vermis (dotted lines) as one median stripe flanked by 3 lateral stripes. Bar = 500 μ m. **D.** Schematic mapping of PrP^{22L} (black areas) shown in **C**. IntP,

interposed cerebellar nucleus; Lat, lateral (dentate) cerebellar nucleus. **E.** Magnification of the inset in **D**. **F.** A banding pattern of PrP^{ME7} similar to that of PrP^{22L} (**E**) is observed in the lobules VI and IV–V of the vermis of a mouse inoculated i.c. **G.** Similar to PrP^{22L} deposits in 22L-infected mice, PrP^{6PB1} deposits surround neurons throughout the dentate nucleus at the clinical stage. **H.** In the cerebellar cortex, PrP^{6PB1} accumulated between the granule cells in the IGL. Note the small plaques of PrP^{6PB1} in the IGL (arrows), ML (arrowheads) and Purkinje cell layer (white arrowhead). Bar = 50 μ m.

Table 1. Parasagittal bands of PrP^{22L} accumulation (grey) and of ZII/AldC-expressing PCs (Z+) throughout the lobules of the cerebellar hemispheres and vermis of the clinically-ill mouse after inoculation of 22L scrapie prions via the i.cb., i.c. and i.p. routes. The maximal number of PrP^{22L} bands observed is given in the grey boxes. PrP^{22L} bands form in the Z+ bands of the vermis and in the Z- bands of the hemispheres. The numbers of parasagittal bands formed by Z+ PCs is given for comparison. PC loss in the Z+ and Z- bands is given in % of the PC linear density in the non infected cerebellum. In most cases, PC loss is the most severe (bold) in the Z- bands. *, intense PrP^{22L} immuno-staining looking homogenous or in vertical palisades; **, Z+ PCs-containing folia; /, not analyzed.

		i.cb.		i.c.		i.p.		ZII/AldC (Z+) bands
		Z+	Z−	Z+	Z−	Z+	Z−	
Lobules		PrP ^{22L} bands						
Vermis	I	*	2			*		3/5
		/	52 ± 24	68 ± 9		/		
	II	*	2			*		9
		/	20 ± 11	58 ± 9		/		
	III	5		7–9		5		9
		49 ± 13	0 ± 5	52 ± 17	60 ± 2	42 ± 13	0 ± 19	
	IV	7		7–11		5		9
		40 ± 8	42 ± 11	45 ± 10	47 ± 10	27 ± 8	56 ± 13	
	V	7		7–11		7		11/13
		40 ± 8	42 ± 11	45 ± 10	47 ± 10	27 ± 8	56 ± 13	
	VI	5		5		3		5/7
		46 ± 10	50 ± 9	53 ± 4	44 ± 13	26 ± 3	49 ± 12	
	VII	5		*		4		4
		/	/	/		/	/	
Hemispheres	VIII	5		5		5–7		7
		72 ± 8	82 ± 10	54 ± 10	74 ± 11	51 ± 14	78 ± 6	
	IX	3		3		3		7
		44 ± 18	52 ± 13	0 ± 10	64 ± 21	30 ± 5	75 ± 9	
	X	1		3		3		**
		0 ± 11	**	0 ± 20	**	11 ± 20	**	
	Sim		2–3		1–3		1	3/5
		74 ± 5	40 ± 11	63 ± 6	68 ± 8	46 ± 25	32 ± 7	
	Crus1		2		2–3		1–2	5
		56 ± 7	48 ± 12	22 ± 19	50 ± 12	0 ± 18	41 ± 3	
	Crus2		3		5		4	6
		92 ± 2	95 ± 2	82 ± 6	93 ± 2	52 ± 13	84 ± 4	
	PM		3		3		5	6
		80 ± 13	91 ± 3	88 ± 4	91 ± 5	55 ± 14	68 ± 14	
Cop		2		2		2	5	
	89 ± 7	88 ± 2	77 ± 7	93 ± 2	59 ± 7	75 ± 12		
PFI	* * *						**	
	/		/		/			
FI	* * *						**	
	/		/		/			
PC loss (%)								

in the paramedian and crus2 folia of the hemispheres in the preclinical period (Figure 1H) and was maintained at the clinical stage in infected mice (Figure 2B). At any given time point, only part of this PrP^{22L} banding pattern was visible in the cerebellum, probably due to inter-individual differences in the time course of the disease thus reflecting the degree of PrP^{22L} propagation in different areas. Aggregated PrP^{22L} from the earliest stripes formed during the preclinical period spread to neighboring and extended regions of the cortex during the clinical period (Figures 1H, 2B, 3A–D).

In the cerebellar cortex of clinically ill mice inoculated i.c. with ME7, the topographic pattern of PrP^{ME7} (Figure 2F) was similar to that displayed by PrP^{22L} (Figure 2E), although the staining of

PrP^{ME7} deposits with the SAF32 anti-PrP antibody was often less intense than that of PrP^{22L} deposits.

By contrast, no PrP^{6PB1} specific topographic pattern was observed in 6PB1 i.c.-infected mice during the clinical period (155–183 dpi). PrP^{6PB1} deposits surrounded the deep cerebellar neurons (Figure 2G). In the cerebellar cortex of these mice, diffuse deposits and small plaques of PrP^{6PB1} were scattered throughout the IGL. Few PrP^{6PB1} plaques were present in the PC and the molecular layers (Figure 2H).

In mice inoculated i.c. either with 22L or ME7, we noticed that the cellular ultrastructure of the cerebellar cortex was most often poorly preserved due to PrP^{TSE}-induced degeneration. Nevertheless,

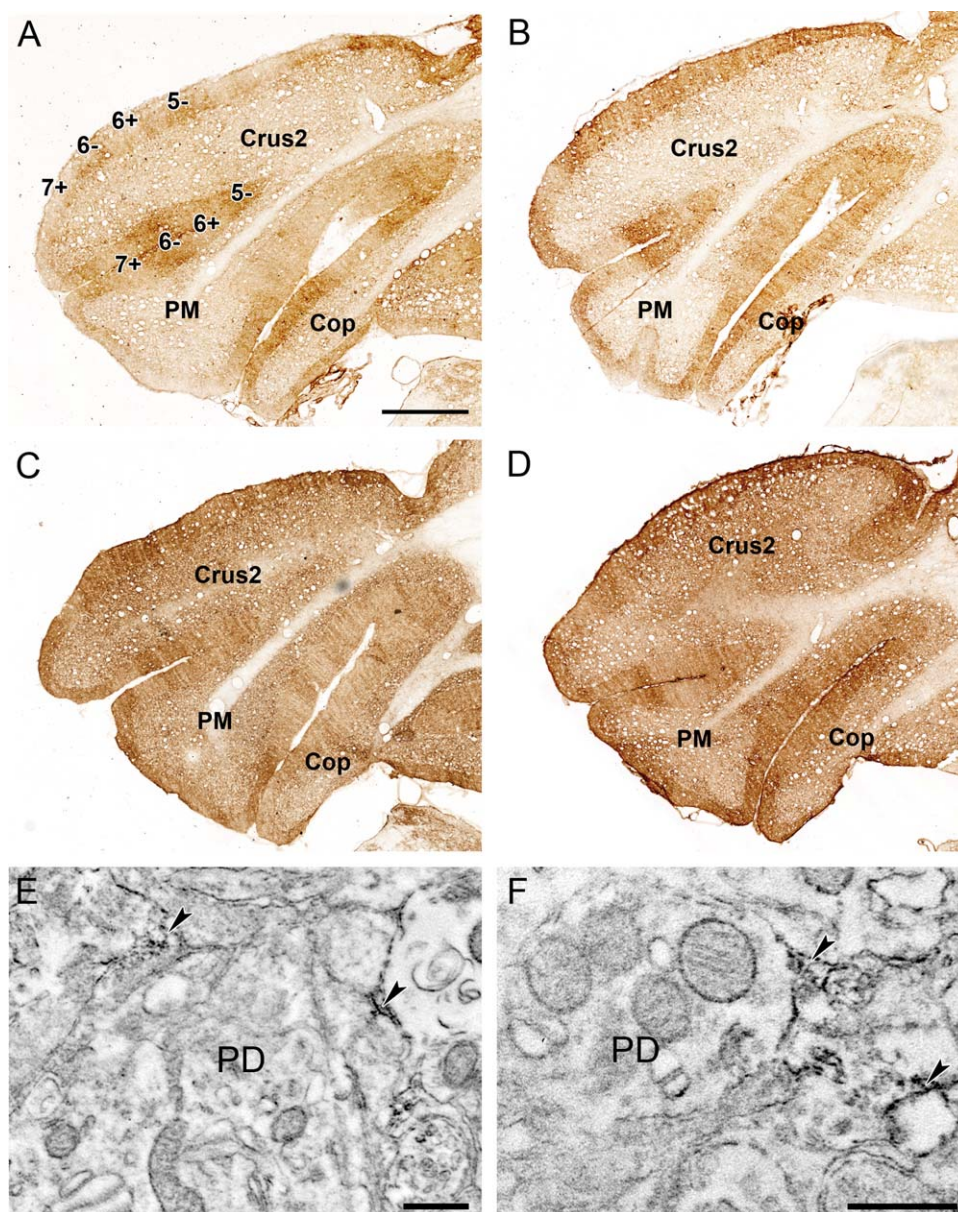


Figure 3. Immunoperoxidase staining of PrP^{22L} and PrP^{ME7} in the cerebellum of clinically ill mice inoculated i.c. **A–D.** Progressive invasion of the cerebellar cortex compartments by PrP^{22L} deposits in the Crus2, paramedian lobule (PM) and copula (Cop) of the hemisphere. See the contrasted striping pattern of PrP^{22L} bands with weakly labeled 6+ and

7+ PrP^{22L}- bands in the earliest stages (A, B) and the increased immunostaining intensity in these regions in the latest stages (C, D). Bar = 500 μm. **E,F.** Ultrastructural localization of PrP^{ME7} in the cerebellar molecular layer. Arrowheads point to stained astrocyte-like profiles closely surrounding remnants of PC dendrites (PD). Bar = 500 nm.

in the few presynaptic profiles observed in PrP+ stripes, PC dendrites and postsynaptic spines were devoid of PrP^{22L} and PrP^{ME7} precipitates, which frequently decorated processes surrounding neuronal profiles (Figure. 3E,F). This most likely corresponded to glial processes, suggesting that astrocytes may participate in PrP^{TSE} production.

These data show that 22L and ME7 scrapie prions but not 6PB1 BSE prions induce a parasagittal banding pattern of PrP^{TSE} aggregation. In addition, production of PrP^{TSE} on astrocyte processes would be associated with the progressive IGL-to-ML prion invasion of the cerebellar cortex.

The PrP^{22L} deposition pattern coincides with spongiosis and loss of Purkinje cells in the cerebellum

To further investigate whether prion-induced histopathology relates to the parasagittal pattern of PrP^{22L} accumulation, we analyzed spongiosis, as well as neuronal loss in the cerebellar cortex of 22L-infected mice.

Vacuolation scores (based on vacuole distribution and density) were determined to establish the lesion profile of 22L scrapie in each part of the cerebellum, using the scale of Fraser and Dickinson

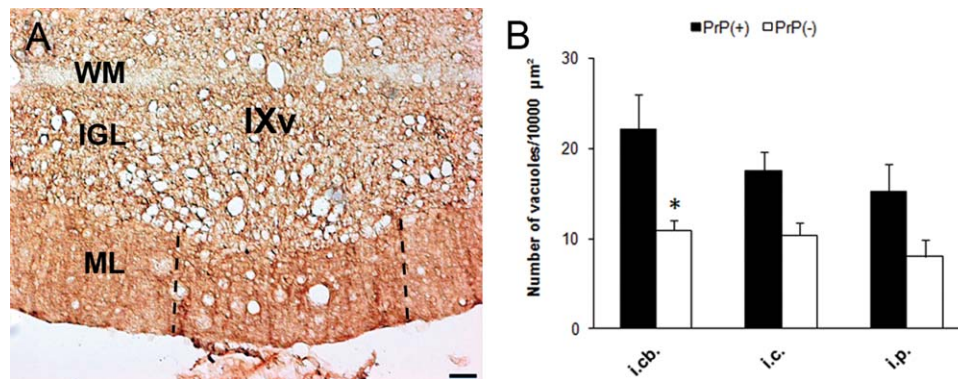


Figure 4. Banding pattern of spongiosis in the cerebellar cortex of 22L-infected mice. **A.** Immunoperoxidase staining of a median stripe of PrP^{22L}+ (between dotted lines) between PrP^{22L}- zones in the cortex of the ventral side of the lobule IX of the vermis. Note the increase in

(44). In mice infected with the 22L strain, only a few, widely and unevenly scattered vacuoles were found in the white matter and deep cerebellar nuclei (score 1). By contrast, robust spongiosis occurred in the neuropil of the cerebellar cortex. At both preclinical and clinical stages of the disease, the most severe spongiosis was observed in the IGL (Figure 4A) and the highest vacuolation score (4), that is, many vacuoles with some confluence, was reached in clinically ill i.cb.-inoculated mice. These lesions significantly increased from the preclinical (0.9 ± 0.1) to the clinical (1.9 ± 0.3) period in the cerebellar cortex ($P < 0.05$), notably in the IGL (1.1 ± 0.2 to 2.4 ± 0.3 ; $P = 0.012$), but did not change significantly in subcortical regions of the cerebellum. Similar lesion scores were estimated in the vermis and the hemispheres in preclinically-ill mice infected i.cb. (vermis 1.0 ± 0.2 , hemispheres 0.9 ± 0.1) and in clinically ill mice infected i.cb. (vermis 1.2 ± 0.2 , hemispheres 1.1 ± 0.2), i.c. (vermis 2.6 ± 0.3 , hemispheres 2.3 ± 0.1) and i.p. (vermis 1.6 ± 0.2 , hemispheres 1.3 ± 0.1). However, in both vermis and hemispheres, vacuolation was significantly more severe in the i.c. than in the i.p. (vermis $P < 0.008$, hemispheres $P < 0.004$) and i.cb. ($P < 0.001$) inoculated mice. In clinically ill 22L-infected mice, the density of spongiosis in the IGL did not significantly differ between PrP^{22L}+ and PrP^{22L}- stripes, but much more vacuoles were found in PrP^{22L}+ stripes in the ML (22.1 ± 3.9 vacuoles/ $10^4 \mu\text{m}^2$) compared with PrP^{22L}- stripes (10.9 ± 1.2 vacuoles/ $10^4 \mu\text{m}^2$) (Figure 4B). Thus, in the 22L-infected cerebellar cortex, severe neuropathogenesis occurs according to the parasagittal banding pattern of PrP^{22L} accumulation with PrP^{22L}+ stripes exhibiting the earliest and most severe spongiosis.

To estimate PC loss, we first counted the number of surviving CaBP-immunolabeled cells in the cerebellum of mock- and 22L-infected mice at the clinical stage of the disease. Approximately half of the total PC population was lost in 22L-infected mice (Figure 5A) and the loss of neurons was not significantly different between the different routes of inoculation in the whole cerebellum. Nevertheless, PC loss was significantly higher in the hemispheres (i.cb. $72.2\% \pm 1.2$; i.c. $68.4\% \pm 6.5$; i.p. $39.5\% \pm 8.3$) than in the vermis (i.cb. $40.7\% \pm 1.9$; i.c. $38.7\% \pm 3.8$; i.p. $32.4\% \pm 4.2$) in all infected mice (i.cb. $P < 0.001$, i.c. and i.p. $P < 0.05$, Figure 6A). PC loss in both the hemispheres and vermis appeared less severe after i.p. inoculation than after i.c. or i.cb. inoculations. Of note,

spongiosis in the ML of the PrP^{22L}+ stripe. IGL, internal granular layer; WM, white matter. Bar = $50 \mu\text{m}$. **B.** The density of vacuoles is increased in the PrP^{22L}+ stripes of the molecular layer in the cerebellum of all infected mice irrespective of the inoculation route (*, $P < 0.05$).

significant PC loss occurred in all lobules, except the lobule X of the vermis and, depending on the inoculation route, a few other folia of the hemispheres (Figure 5B). Nevertheless, two-way (lobule, inoculation route) ANOVA followed by *post hoc* Tukey tests showed that PC linear densities were not significantly different in any of the cerebellar lobules between the i.c., i.cb. and i.p. inoculation routes.

We further explored the impact of prion infection on other neuronal populations of the cerebellar cortex in 22L clinically ill mice. In the IGL, the granule cell density was generally unaffected, and there was no difference in granule cell densities between cerebellar PrP^{22L}+ (19337 ± 1181 granule cells/ mm^2) and PrP^{22L}- (19403 ± 594 granule cells/ mm^2) stripes in i.c. inoculated mice ($P = 0.948$). A moderate, but significant granule cell loss was however found in i.cb. ($21.9\% \pm 5.7$, $P < 0.01$) and i.c. ($18.5\% \pm 3.3$, $P < 0.05$), but not in i.p. ($11.5 \pm 3.9\%$, $P = 0.393$) inoculated mice. Concerning interneurons of the ML, their density did not significantly evolved (sham 279 ± 66.2 ; $P = 0.456$) in mice inoculated i.cb. (300.5 ± 31.2 interneurons/ mm^2), i.c. (351.9 ± 25.2 interneurons/ mm^2) or i.p. (368 ± 25.1 interneurons/ mm^2).

Importantly, at the preclinical period (107 dpi), CaBP-immunolabeled PCs primarily disappeared in PrP^{22L} accumulation zones (Figure 5C,D) with 90.7% loss (3.6 PCs/mm) in PrP^{22L}+ stripes and 27.9% loss (28.3 PCs/mm) in PrP^{22L}- stripes ($n = 1$). Loss of PCs in the 22L-infected cerebellum likely depended on apoptotic mechanisms as some CaBP-labeled PC somata were labeled for activated caspase-3 (Figure 5E). PC loss then continued throughout the clinical course of the disease (Figure 5F,G) with 68.2% loss (12.5 PCs/mm) in PrP^{22L}+ stripes and 7.8% loss (36.2 PCs/mm) in PrP^{22L}- stripes ($n = 1$). Quantitative analysis of PC loss performed with i.c. inoculated mice ($n = 3$) revealed that nearly all PCs disappeared from the PrP^{22L}+ stripes ($86.3 \pm 10\%$ loss; 3.7 ± 2.7 PCs/mm) by the clinical period, while about 3.5 times more PCs were still present in PrP^{22L}- stripes ($47.7 \pm 17.1\%$ loss; 14.2 ± 4.7 PCs/mm). Although this difference was not significant for the whole cerebellum, PC loss was significantly greater in the PrP^{22L}+ stripes than in the PrP^{22L}- stripes in the hemispheres, but not in the vermis (Figure 6B).

Altogether, our data clearly indicate that Purkinje cells are the neuronal cells most vulnerable to 22L prion toxicity with a massive PC loss in PrP^{22L}+ stripes.



Figure 5. PC loss in the cerebellum of 22L-infected mice. **A,B.** Decreased linear densities of PCs in the cerebellum (A) and cerebellar lobules (B) of clinically ill mice inoculated i.cb. (A, B), i.c. and i.p. (A) with 22L prions. PC loss is similar, irrespective of the inoculation route (i.c. $55.4\% \pm 4.9$; i.cb. $63.0\% \pm 3.3$; i.p. $50.4\% \pm 5.6$). All lobules of the vermis and hemispheres except the lobule X of the vermis exhibit significant PC loss. **C,D.** Arrow points to a narrow PrP^{22L} stripe labeled by immunoperoxidase in C, and in the green channel in D where CaBP immunofluorescence (red channel) shows that some PCs are already lost in crus2 at a preclinical stage (107 dpi) of the disease (22L i.cb.). **E.** Merged image of immunofluorescence of active caspase-3 (green channel) and CaBP (red channel) showing apoptotic PCs (arrows, and at higher magnification in inset) in the cerebellar cortex of a clinically ill (134 dpi) mouse inoculated i.cb. **F,G.** In clinically ill (134 dpi) mice inoculated i.cb., merged images of PrP^{22L}

immunoperoxidase (green channel) and CaBP immunofluorescence (red channel) showing the loss of PCs in PrP^{22L} stripes in the IV–VI lobules (F) and in the paramedian lobule (PM) and copula pyramidis (Cop) (G). **H.** The decrease in the linear density of zebrin-PCs (EAAT4+ or aldolase C+) is less than the decrease in zebrin–PCs in the cerebellum of all clinically ill 22L-inoculated mice compared with sham/mock-infected mice. A, B, H. $*P < 0.05$; $**P < 0.001$; $\#P < 0.05$. **I.** Merged image of EAAT4-eGFP (green channel) and CaBP immunofluorescence (red channel) showing 5+ and 6+ stripes of EAAT4+ PC (yellow) and a 5– stripe of EAAT4– PCs (red channel) in the crus2 and PM of a mock-infected EAAT4-eGFP mouse. **J,K.** In crus2 and PM of a clinically ill (139 dpi) EAAT4-eGFP mouse inoculated i.c., most of the surviving CaBP+ PCs (J, red) are present in the 5+ and 6+ stripes of EAAT4+ PCs (yellow) shown in merged image K and not in the 5– stripe of EAAT4– PCs. C–G, I–K. Bar = 50 μ m.

$25.6\% \pm 4.4$ vs. EAAT4–: $50.1\% \pm 8.6$) 22L-infected mice ($P < 0.001$). With i.cb.-inoculated mice, the loss of EAAT4+ PCs was not significantly different from that of EAAT4– PCs. Nevertheless, EAAT4+ PC loss in the cerebellum of i.cb.-inoculated mice was higher ($57.1\% \pm 6.9$) than that measured with i.c.

($41.4\% \pm 5.2$, $P = 0.938$) and i.p. ($25.6\% \pm 4.4$, $P = 0.001$) inoculated mice.

These data indicate that zebrin expression in specific subpopulations of cerebellar Purkinje cells is associated with some PC resistance to prion toxicity.

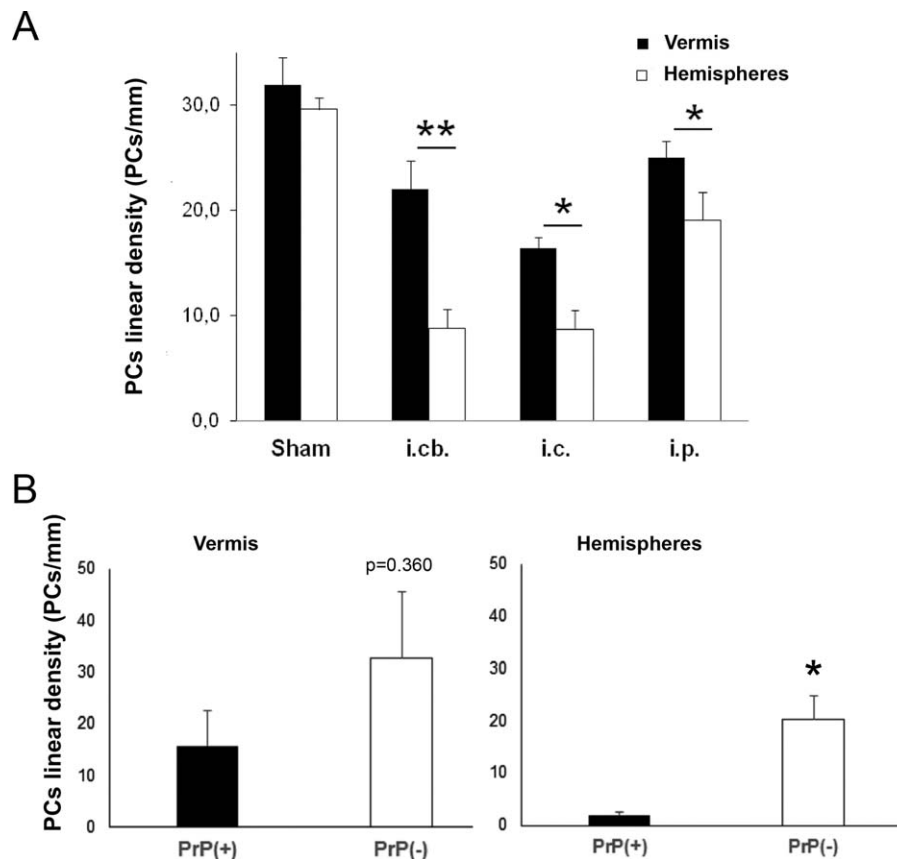
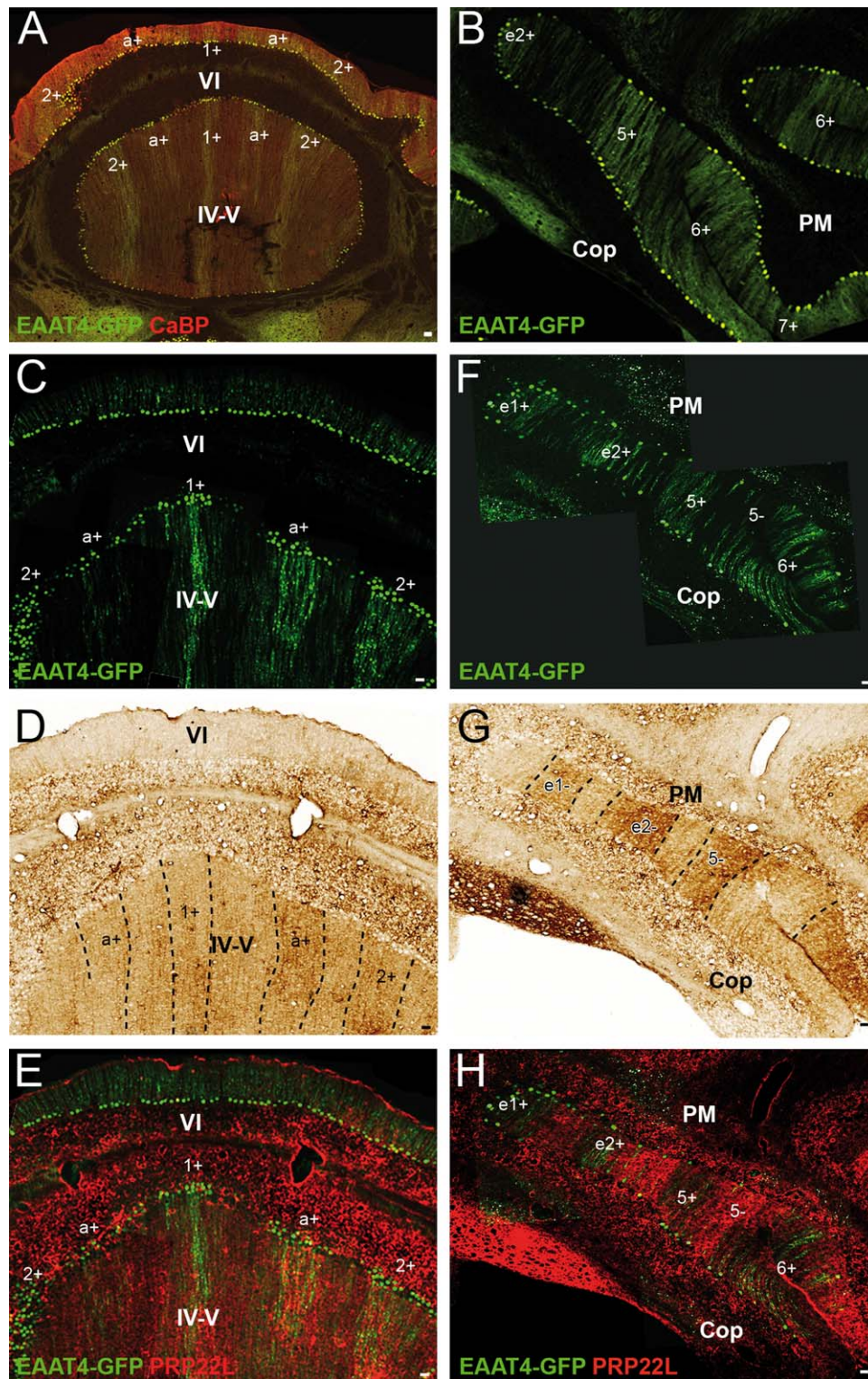


Figure 6. **A.** Variable severity of PC loss in the cerebellar vermis and hemispheres between the i.cb., i.c. and i.p. inoculation routes of 22L scrapie as reflected by differential decrease in PC linear density. $*P < 0.05$; $**P < 0.001$. **B.** PC loss between PrP^{22L}+/PrP^{22L}– bands

in the vermis and the hemispheres of clinically ill i.c. inoculated mice. PC loss is significantly more severe in the PrP^{22L}– bands in the hemispheres ($*P < 0.05$).



PrP^{22L} accumulates in Z⁺ bands of the vermis and in Z⁻ bands of the hemispheres

We next probed whether the PrP^{22L} banding pattern in the cerebellar cortex of 22L-infected mice fully matches with the banding

pattern of EAAT4 and ZII/AldC zebrins-expressing Purkinje cells. Although the parasagittal EAAT4 or aldolase C zebrin pattern was somewhat blurred by PC loss in 22L-infected mice, the PrP^{22L} deposition pattern in single and consecutive sections of the

Figure 7. Banding patterns of EAAT4-eGFP and PrP^{22L} in the median level of the cerebellum (A, C-E, bregma -6.64; B, F-H, bregma -6.72) of sham (A, B) and clinically ill (203 dpi), 22L i.p. inoculated (C-H) mice. **A,B.** In the cerebellum of the mock-infected EAAT4-eGFP mouse, the stripes of the EAAT4-eGFP PC subpopulation (green channel) which coincide with CaBP immunostained PCs (red channel) are indicated in yellow in the merged image of the vermis (A) and the stripes of EAAT4-eGFP PCs are seen in the paramedian lobule (PM) and copula pyramidis (Cop) (B) of the hemisphere. **C-E.** In the cerebellum of a diseased EAAT4-eGFP mouse presented at a level similar to the vermis

shown in A, stripes of green fluorescent EAAT4-eGFP PCs (C) coincide with stripes of immunoperoxidase labeled deposits of PrP^{22L} (between dotted lines in D). In the merged image (E) of C and D, PrP^{22L} staining is visualized in the red channel. 1+, a+, 2+, parasagittal stripes of EAAT4-eGFP+ PCs in the lobules VI and IV-V of the vermis. **F-H.** In PM and Cop of the cerebellar hemisphere, immunoperoxidase stained PrP^{22L} stripes (dotted lines in G, red channel in merged image in H) coincide with stripes of EAAT4-eGFP+ PCs (F, H). e1+, e2+, 5+, 5-, 6+, parasagittal stripes of PCs expressing (+) and non-expressing (-) EAAT4-eGFP in PM and Cop. Bar = 50 μ m.

cerebellar cortex closely corresponded to the EAAT4 and ZII/aldC zebrins patterns (Figure 7, Table 1). During the clinical course of the disease (139–145 dpi), this was particularly clear in the lobules III–VIII of the vermis. In these lobules, there was nearly perfect overlapping of PrP^{22L} stripes with the 1+, a+, 2+, 3+ and 4+ stripes of EAAT4+ PCs, while the EAAT4- 1-, a-, 2- and 3- stripes were only weakly stained for PrP^{22L} (Figure 7A,C–E). However, three PrP^{22L} stripes were observed in the IXth and Xth lobules of the vermis, which contains almost exclusively EAAT4+ PCs (Figure 8). CaBP immunostaining as well as EAAT4 fluorescence disclosed a decreased PC density in these areas (Figure 9). By contrast, a reversed correspondence was observed in the hemispheres. The parasagittal stripes of robust PrP^{22L} accumulation occurred in the e1-, e2-, 5- and 6- stripes containing EAAT4- PCs and crossed into the crus2, paramedian and copula pyramidis folia, while the adjacent EAAT4+ stripes displayed much weaker if any PrP^{22L} immunostaining (Figure 7B,F–H).

These overall data show that the parasagittal banding pattern of PrP^{22L} precipitation in the mouse cerebellar cortex is similar to the organizational pattern of PC subpopulations disclosed by zebrin expression. Although PrP^{22L} accumulates both in Z+ bands of the vermis and in Z- bands of the hemispheres, Z- PCs are by far the most sensitive neuronal cells to 22L prion toxicity. Since Z- PCs are lost in and out the PrP^{22L} bands, Z- membership rather than PrP^{22L} is likely to promote PC death.

Prominent microgliosis and astrogliosis occur in PrP^{22L}+ bands

The activation of microglial cells and astrocytes is an early component of the brain response to prion infection, known to aggravate neurodegeneration by exacerbating neuroinflammation (16, 28, 49, 73, 81, 94). To further explore whether the loss of PCs in PrP^{22L}+ stripes would also depend on microglia, we examined the activation state of microglial cells and astrocytes in cerebellar sections of 22L-infected mice.

Immunolabeling of Iba-1 to detect activated microglial cells revealed that the density of active microglial cells dramatically increased throughout the cerebellar cortex of clinically ill 22L-infected mice (329.2 ± 26.1 cells/mm², $n = 4$ mice inoculated i.c./ 33.3 cells/mm², $n = 1$ sham mouse, data not shown) with a significant peak in PrP^{22L}+ stripes (427.7 ± 54.0 cells/mm²) compared with the PrP^{22L}- stripes (230.7 ± 32.6 cells/mm²) (Figure 10A).

Contrasting with the presence of reactive microglia throughout the infected cerebellum, the astrocyte response to 22L prions was restricted to patches of intensely GFAP-labeled astrocyte processes and Bergman palisades in the IGL and the ML of the cerebellar

cortex, respectively (Figure 10B–D). Double immunohistochemistry for GFAP and PrP^{22L} revealed the topographic coincidence of astrogliosis and PrP^{22L} patterns with reactive astrogliosis occurring in PrP^{22L}+ stripes (Figure 10D).

Correlation between prion-induced perisynaptic astrocyte activation and TNFR1 upregulation

Reactive astrogliosis in neurodegenerative diseases is often associated with the release of pro-inflammatory factors such as TNF- α

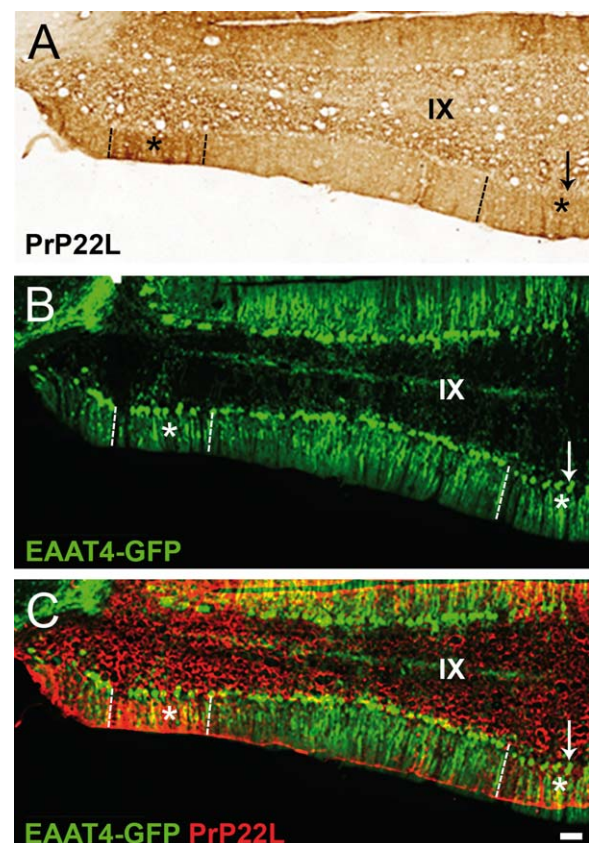


Figure 8. PrP^{22L} banding pattern and PC loss in the IXth lobule of the cerebellar vermis of a clinically ill (235 dpi) mouse inoculated i.p. with 22L prions. **A.** Asterisks show a lateral and a median PrP^{22L} bands labeled with immunoperoxidase. **B.** The PCs of the lobule IX are all labeled with EAAT4-GFP green fluorescence (green channel). **C.** The merged image shows decreased density of fluorescent PCs (green channel) in the PrP^{22L} bands (red channel). Arrow shows the median line. Bar = 50 μ m.

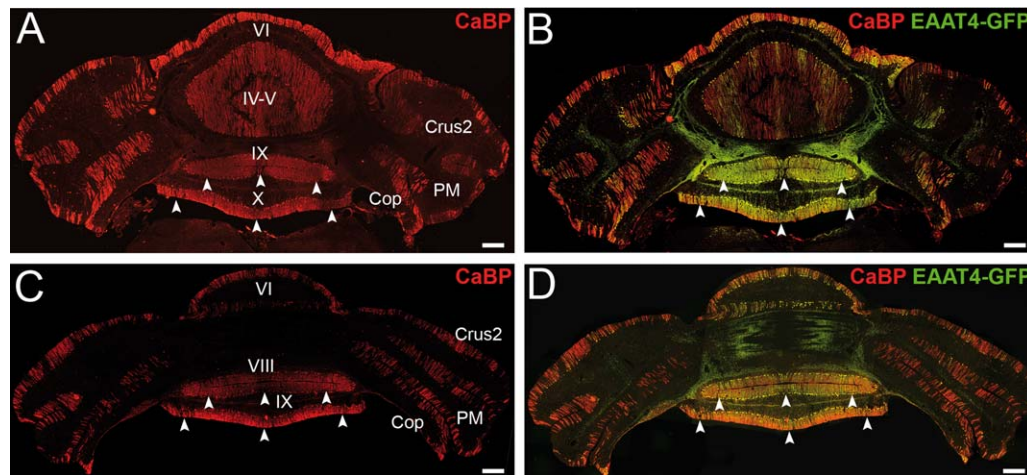


Figure 9. PC loss in the cerebellum of clinically ill 22L-infected EAAT4-GFP mice. Merging CaBP-immunofluorescence (**A,C**, red channel) and EAAT4-GFP fluorescence (**B,D**, green channel) images of cerebellar sections in the median (**A, B**, bregma -6.72 mm) and posterior (**C, D**, bregma -7.20 mm) cerebellum after i.c. (139 dpi) and i.p. (205 dpi) inoculation. At both levels, most of the surviving CaBP-

immunofluorescent PCs (red in **A** and **C**) are EAAT4-GFP expressing PCs (orange-yellow in **B** and **D**). PC loss is less severe in the vermis which contains a majority of resistant EAAT4-GFP PCs. Arrowheads show bands of decreased density of PCs in the IXth (**A–D**) and Xth (**A, B**) lobules of the vermis. Bar = $500\ \mu\text{m}$.

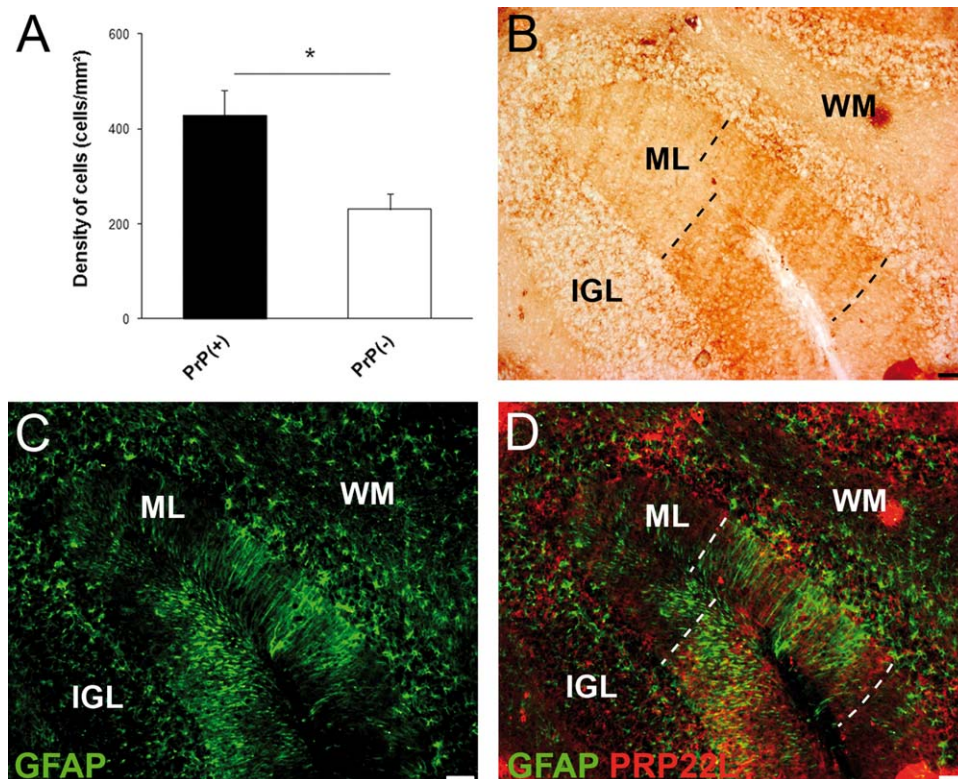


Figure 10. Inflammation patterns in the 22L-infected cerebellum. **A.** In the cerebellar cortex of clinically ill mouse inoculated i.c., the density of reactive microglia immunostained for Iba-1 in the molecular layer is significantly higher in PrP^{22L}+ stripes than in PrP^{22L}- stripes ($*P < 0.05$). **B,C.** Immunoperoxidase staining of PrP^{22L} (**B**) and immunofluorescence of GFAP (**C**) in PM and Cop of the cerebellum of a

clinically ill mouse inoculated i.c.b. **D.** Merged image of **B** (red channel) and **C** (green channel) showing enhanced GFAP fluorescence of astrocytes in PrP^{22L}+ stripes (between dotted lines in **B** and **D**). The CaBP immunofluorescent PCs are shown in the PrP^{22L}- stripes of the same region in Figure 5G. IGL, internal granular layer; ML, molecular layer, WM, white matter. Bar = $50\ \mu\text{m}$.

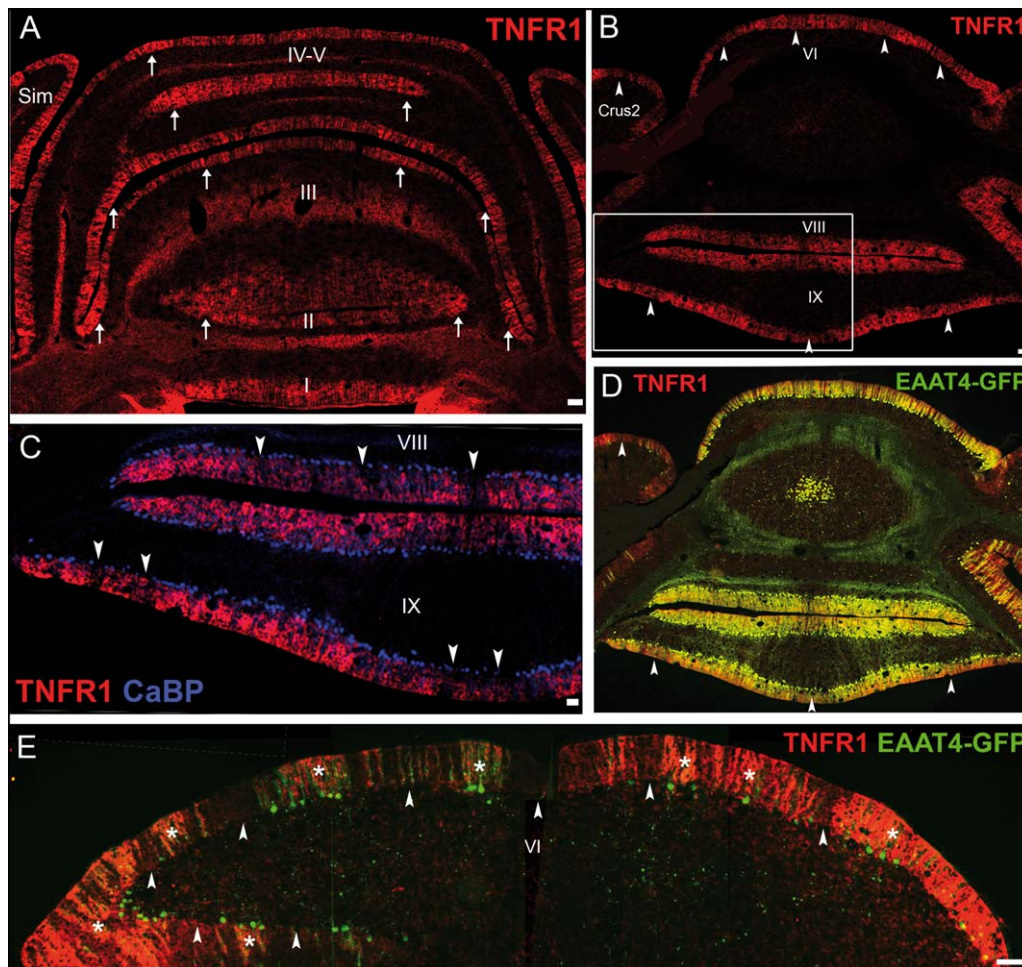


Figure 11. TNFR1 immunostaining in the vermis of the anterior (**A**, bregma -5.68 mm) and posterior (**B–E**, bregma -7.20 mm) cerebellum of clinically ill EAAT4-GFP transgenic mice inoculated i.c. with 22L prions. **A**. TNFR1 immunofluorescent stripes (arrows) and palisades in the anterior lobules V to I. **B**. TNFR1 immunofluorescent stripes and palisades alternate with immunonegative stripes (arrowheads) in the VI, VIII and IX lobules. **A**, **B**, bars = $200\ \mu\text{m}$. **C**, **D**, **E**. Merged images of TNFR1 (red channel) and CaBP (**C**, blue channel) or

EAAT4-GFP (**D**, **E**, green channel) show TNFR1 immunofluorescent stripes and palisades (**C**, pink; **D**, yellow; **E**, orange-red, asterisks) overlapping the surviving PC dendrites in the cerebellar molecular layer. **C**. Magnification of inset in **B**. The linear density of the surviving CaBP immunofluorescent PCs (**C**, blue) and EAAT4-GFP fluorescent PCs (**D**, **E**, green) is visibly decreased in the TNFR1 immunonegative stripes (arrowheads). **C**, **E**, bars = $50\ \mu\text{m}$.

(124). Interestingly, upregulation of the TNF- α receptor type 1 (TNFR1) (27, 95, 107) has been shown in the cerebellum of 22L-infected mice, which might accelerate the neurodegenerative process in response to prion-induced release of TNF- α . Of note, TNFR1 accumulation follows a parasagittal banding in the ML (95) that recalls the parasagittal banding pattern of prion pathogenesis in the cerebellar cortex. To shed further light on the structures concerned by TNFR1 accumulation in prion-infected cerebellum, we first compared the TNFR1 accumulation and PrP^{22L} precipitation patterns. In mock-infected mice, a weak TNFR1 immunostaining was detected in the deep cerebellar nuclei and throughout the ML of the cerebellum (data not shown). TNFR1 staining intensified in the preclinical period in the cerebellar hemispheres of mice inoculated i.c.b. with 22L prions. Intensely stained TNFR1+ regions were bracketed by unstained palisades (data not shown) and by the clinical stage, TNFR1+ palisades and stripes were observed

throughout ML in all infected mice (Figure 11A,B). The PrP^{22L} and TNFR1 immunostaining patterns were complementary with PrP^{22L} accumulating between TNFR1 palisades and stripes (Figure 12A,B). Estimating PC survival throughout the banding pattern of TNFR1 in infected mice showed that CaBP-stained PCs, including EAAT4+ PCs and, to a lesser extent EAAT4– PCs, survived in TNFR1+ palisades and stripes (Figures 11D,E and 12C–H). Nevertheless, TNFR1 and CaBP were not consistently co-localized as the dendritic spines of CaBP-stained PCs were usually surrounded by TNFR1 immunofluorescent dots (data not shown). This suggests that TNFR1 was not located on PC processes in clinically ill 22L-infected mice. Since the vGLUT1-immunostained presynaptic terminals of parallel fibers were distributed uniformly in the ML of both clinically ill and non-infected mice, which thereby excludes parallel fiber boutons as the preferred sites of increased TNFR1 expression (data not shown), we examined the possibility

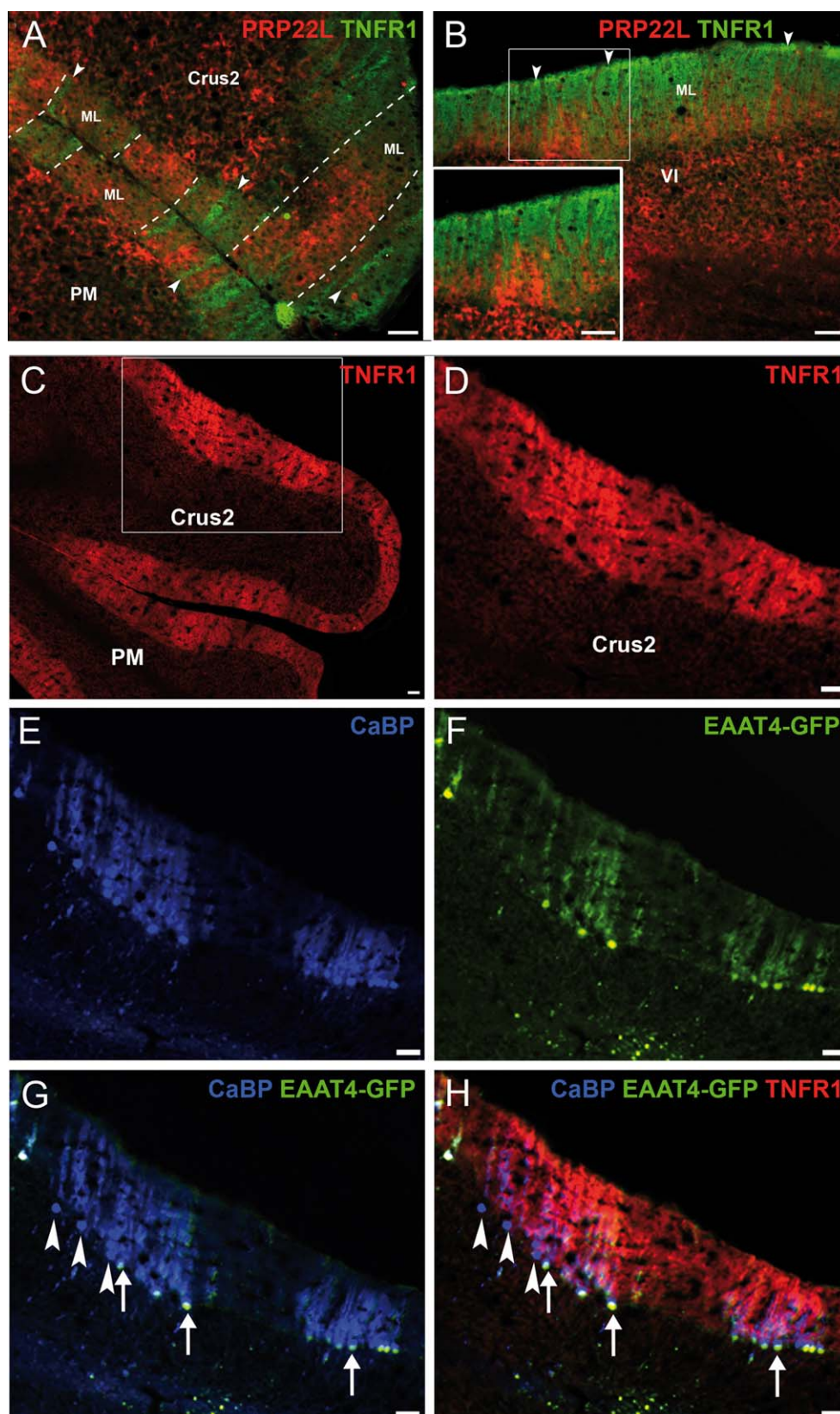


Figure 12. TNFR1 increases in PrP^{22L}– stripes where PCs survive. **A,B.** Merged images of TNFR1 (green channel) and PrP^{22L} (red channel) immunofluorescence in PM (A) and Vlt lobules (B) from a clinically ill (134 dpi) mouse inoculated i.c.b. TNFR1 is enhanced in PrP^{22L}– stripes (between dotted lines in A) and palisades (arrowheads). Inset shows higher magnification of PrP^{22L} deposits and TNFR1 staining. Bar=50µm. **C,D.** Immunofluorescence of TNFR1

stripes (red channel) in the ML of crus 2 and PM of a clinically ill (145 dpi) mouse inoculated i.c. with 22L. D–H. Magnification of inset in A. **E–H.** Immunofluorescence of CaBP (blue channel, E) and EAAT4-eGFP (green channel, F) and in merged image of E and F zebrin+ (yellow, arrows) and zebrin- (blue, arrowheads) PCs are visualized (G). H. Merged image of D and G. TNFR1 immunofluorescence (red) is associated with both types of PCs. Bar = 50 µm.

that these sites were non neuronal components of the ML such as the astrocytes. The patterns of TNFR1 and GFAP-labeled astrogliosis were clearly distinct, but complementary in the ML of infected mice (Figure 13A–C). TNFR1 and the glial glutamate transporter EAAT1 appeared however to localize on the same structures in the ML of the 22L-infected mice (Figure 13D). An ultrastructural examination of this region revealed TNFR1 immunoperoxidase staining at the plasma membrane of distal astrocyte processes surrounding asymmetrical PC-parallel fiber synapses (Figure 13E,F). Interestingly, the most intense labeling occurred close to the postsynaptic component of the synapses, that is, the PC dendritic spines (Figure 13E,F).

These results provide evidence that the glial response to prion invasion is closely circumscribed by the parasagittal banding pattern of pathogenesis in the cerebellar cortex (Figure 14). In addition to the increased density of activated microglia in the PrP^{22L}+ bands, the increase in GFAP+ astrocytes in these bands and the up-regulation of TNFR1 expression at astrocyte tips enveloping PC postsynaptic spines in PrP^{22L}– bands suggest a biphasic reaction of astrocytes during prion disease.

DISCUSSION

The scrapie strain property and the cerebellar compartmentation, but not the neuroinvasion route, determine the pattern of PrP^{22L} accumulation

The present anatomical analysis provides evidence that both scrapie PrP^{22L} and PrP^{ME7} precipitate according to a parasagittal banding pattern in the mouse cerebellum, as previously documented (4, 20, 61, 95), while the 6PB1 bovine strain displays a random accumulation pattern. Although there is substantial evidence that prions spread to the cerebellar cortex along well defined, synaptically linked neural pathways (10, 11, 17, 111, 126), we here show that the neuroinvasion route does not however impact on the banding patterns of PrP scrapie deposits.

For instance, PrP^{TSE} distribution in the central nervous system and PrP^{TSE}-induced cerebellar neuropathology have been shown to be mainly influenced by the molecular features of PrP^{TSE} as well as polymorphism and mutations of the cellular prion protein encoding gene *PRNP* (50, 70, 71, 84, 91, 109, 123). The differential deposition of PrP^{22L} and PrP^{ME7} across the parasagittal organization of Purkinje Cell (PC) modules indicates here that a local “compartmentation parameter” also modulates pathogenesis of 22L and ME7 scrapie prions and possibly CJD. Of note, bands of PrP^{22L} aggregates start to appear in the IGL before invading adjacent ML areas, suggesting that the cortical compartmentation of

PrP^{22L} accumulation occurs in both the IGL and ML and that cells of the IGL are intrinsically more responsive to prion infection.

With time, the sustained production of PrP^{TSE} leads to the complete invasion of the cerebellar cortex, as revealed by the progressive disappearance of PrP^{22L} stripes. Cell-specific differences, such as variations in the PrP^C glycosylation profile between cells targeted by prions, might modulate the interaction between PrP^{TSE} and the host PrP^C, at the root of regional differences in the rate of PrP^{TSE} production (13, 30, 31, 130).

Purkinje cells are major targets of 22L prions

We show significant loss of PCs, but not of cortical interneurons, in the cerebellum of prion-infected mice, indicating that PCs are the main neuronal targets of 22L scrapie. As PCs are the sole efferent projections of the cerebellar cortex and extensive PC death was shown to impact on motor coordination, cerebellar learning, and to provoke ataxia (100), the targeting of 22L prions to PCs likely accounts for the ataxia observed in the scrapie-diseased mice. Comparison of PC survival between the PrP^{22L}+ and PrP^{22L}– stripes throughout the cerebellar cortex revealed that PC loss occurred in the PrP^{22L}+ stripes in the preclinical period, and conversely more PCs survived in the PrP^{22L}– stripes all along the course of the disease. In addition, vertical palisades of PrP^{22L} formed in regions of the ML where the dendrites of PCs, but not the soma, have degenerated, arguing that PrP^{22L} accumulation starts at the dendrites (116). Remarkably, PrP^{CJD} deposits are also closely associated with cerebellar cell dendrites (74). The clustering of PrP^{CJD} deposits in the ML may reflect some loss of individual PCs but also degenerative processes that affect other surrounding components in the ML, such as terminals of afferent fibers (5) or Bergmann astrocytes (see below). Our observations however confirm that granule cells and parallel fibers are resistant to 22L prions neurotoxicity (116).

The topographic coincidence of PrP^{22L} accumulation and PC loss is consistent with the spatial overlap of PrP^{TSE} and neurodegeneration observed in several other murine models of prion disease (41, 86, 88, 129). Spongiosis was extensive in the ML of the PrP^{22L}+ stripes and even more throughout the IGL where a robust PrP^{22L} accumulation occurred at the clinical stages of the disease, suggesting a coupling between PrP^{22L} accumulation and neurotoxicity. Contrasting with this hypothesis is our observation of a significant PC loss in PrP^{22L}– stripes associated with little to moderate neuronal loss in the PrP^{22L}-enriched IGL. In the IGL of sCJD patients, granule cell loss is also negatively correlated with PrP^{TSE} accumulation (22, 37, 132) and uncoupling between high prion infective titers and neurotoxicity has recently been demonstrated (102).

Although the global loss of PCs was not significantly different between clinically ill mice inoculated i.c., i.c.b. and i.p., the i.c. route induced the most severe vacuolation and PC death than the

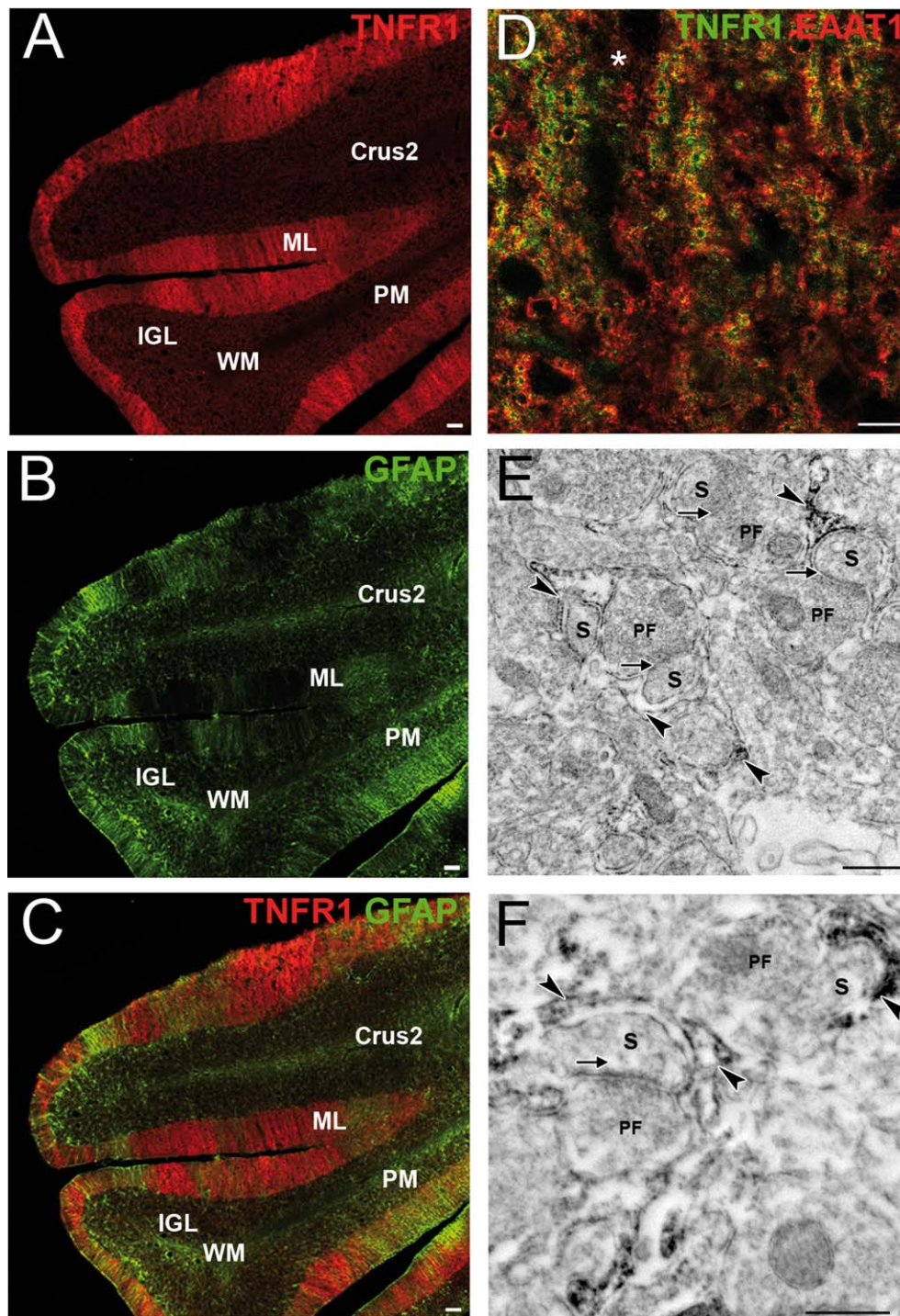


Figure 13. Subcellular localization of TNFR1 in the cerebellar ML of clinically ill (139 dpi) mice inoculated i.c. **A–C.** Complementary immunofluorescence patterns of TNFR1 (red channel, A) and GFAP (green channel, B) stripes and palisades in the ML of crus 2 and PM of a clinically ill (145 dpi) mouse inoculated i.c. C. Merged image of A and B. GFAP immunofluorescent palisades of Bergman astrocytes are present in the stripes and palisades displaying weak TNFR1 immunofluorescence. Note also the reactive GFAP astrogliosis in the

IGL and WM. Bar = 50 μ m. **D.** Merged confocal image showing partial co-localization (yellow) of TNFR1 (green channel) and EAAT1 (red channel). Row with weak immunofluorescence is indicated by *. Bar = 10 μ m. **E,F.** Transmission electron micrographs of preembedded immunoperoxidase staining of TNFR1 in the ML neuropil. Perisynaptic astrocyte processes (arrowheads) bear the most of immunoperoxidase staining close to PC spines (S) establishing asymmetrical synapses (arrows) with parallel fiber boutons (PF). Bar = 500 nm.

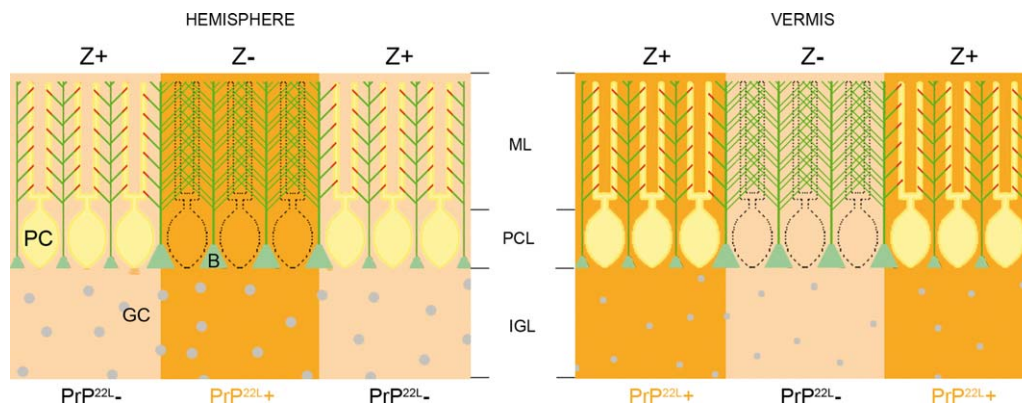


Figure 14. Schematic representation of prion-induced pathogenesis in cerebellar compartments. PrP^{22L} aggregates (dark orange) in ML, PCL and IGL in the bands made by Z⁻ PCs of the vermis and in the bands made by Z⁺ PCs of the hemisphere. Bergmann astrocytes (B) gliosis

extends over lost Z⁻ PCs (dashed outline). The tips of Bergmann astrocyte processes (red) express TNFR1 close to the dendrites of surviving Z⁺ PCs. GC, granule cell (blue).

other routes in the vermis and the hemispheres. This suggests that the rate and/or intensity of scrapie pathogenesis might be increased after neuroinvasion by the i.c.-related intracerebral pathways. Such a link between the severity of pathogenesis and the neuroinvasion pathways is however difficult to establish. As the amounts of 22L prions and the starting time-point of cerebellum neuroinvasion by 22L prions by i.c. and i.p. inoculation routes cannot be precisely determined, our comparative analysis of the three neuroinvasion routes (i.c., i.p., i.cb.) did not allow to determine whether differences in severity of pathology, that is, PC loss, spongiosis and PrP^{22L} accumulation, originate from an asynchrony between the disease courses or from different pathogenic mechanisms.

Our results indicate that spongiosis and death of PCs, the most sensitive neurons to 22L prions in the cerebellar cortex, preferentially occurs in the PrP^{22L} stripes in the ML while granule cells resist to 22L prions in spite of enhanced spongiosis and PrP^{22L} precipitation in the subjacent IGL. This indicates uncoupling between PC loss and the accumulation of PrP^{22L}, and suggests that other cell types than PCs such as Bergmann astrocytes or granule cells contribute to PrP^{22L} production.

The stripe-like accumulation of PrP^{TSE} in the cerebellar cortex recalls the structure of modular compartments in the cerebellum (58) and the topography of PrP^{22L} stripes corresponds to that of PCs stripes defined by the expression of EAAT4 and ZII/AldC zebrins in most of the folia of the cerebellar vermis and hemispheres. This reveals that a host parameter linked to the cerebellar compartmentation restricts 22L scrapie pathogenesis. Whatever the intra- or extracerebellar route of inoculation, a similar parasagittal banding pattern of PrP^{22L} was observed, indicating that the host factor involved is not related to the extracerebellar organization of PCs connectivity. Intriguingly, PrP^{22L} stripes overlapped with zebrin⁺ (Z⁺) PC stripes in the vermis, but with zebrin⁻ (Z⁻) PC stripes in the hemispheres. This inverted coincidence of PrP^{22L} and zebrin expression supports the view that the modular pattern of the cerebellar cortex rather than the biochemical properties of these PC subpopulations, dictates the topography of PrP^{22L} accumulation. Although this cannot be satisfactorily explained, similar differences between vermal and hemispheric zebrin expression patterns have

been previously reported (7). We cannot formally exclude that a yet-to-be identified factor common to these PC subpopulations is at the root of the topographic deposition of PrP^{22L}.

In the hemispheres, PC loss is significantly greater in the PrP^{22L}⁺ bands (ie, prion sensitive Z⁻ PCs bands) than in the PrP^{22L}⁻ bands (ie, prion resistant Z⁺ PCs bands). In the vermis, PrP^{22L} accumulates in the resistant Z⁺ PCs bands. However, the loss of Z⁺ PCs in the PrP^{22L}⁺ bands in the vermis is less than the loss of Z⁻ PCs in the PrP^{22L}⁺ bands of hemispheres. The loss of PCs would rather concern the Z⁻ subpopulation of these neurons. This suggests that PC death is related to Z⁻ membership rather than PrP^{22L} accumulation. Scrapie is the first pathology described that alters cerebellar patterns differentially in the vermis and hemispheres. Nevertheless, the only pathologic feature that differs between the two regions is the pattern of PrP^{22L} bands, that is, the topography of PrP^{22L} accumulation, the Z⁻ PCs being more sensitive than Z⁺ PCs throughout vermis and hemispheres. This suggests that cerebellar compartmentation is a topographic parameter of PrP^{22L} accumulation in the mouse cerebellum.

Of note, more Z⁻ PCs than Z⁺ PCs have been lost in the cerebellar cortex of 22L-infected mice at the clinical stage of the disease, suggesting that those PCs expressing the zebrins EAAT4 and ZII/AldC are less vulnerable to prion toxicity. However, many more Z⁺ PCs were lost in mice inoculated directly in the cerebellum (i.cb.) and the differential sensitivity of the PCs subpopulations to prion toxicity was less pronounced in those mice when compared with the i.c. and i.p. inoculated mice. Although more resistant, the direct inoculation of prions into the cerebellum might have precipitated the death of Z⁺ PCs by skipping the pre-cerebellar neuroinvasion step.

In most diseases affecting PCs, the ZII/AldC- PC die first (9, 14, 39, 40, 89, 105, 106, 119) although other scenarios have been observed (35, 36, 112, 113) suggesting that the pattern of cell death in the cerebellum does not only depend on the higher sensitivity of one peculiar PC subpopulation to toxic insult, but rather implies specific death pathways (104). In prion diseases, the enhanced vulnerability of Z⁻ PCs to 22L scrapie may be associated with excitatory inputs originating from climbing and mossy fibers and the

high density of calcium channels (125) and glutamate receptors (14, 83, 108) in Z[−] PCs. Extended survival of Z⁺ PCs would instead relate to the expression of EAAT4 and ZII/AldC that permit to satisfy energy demands and resist excitotoxicity (33). In addition, loss of PrP^c protective functions toward neuron excitability (38) and excitotoxicity (26) upon its conversion into PrP^{TSE} would also contribute to the improved vulnerability of specific PCs subpopulations infected by prions.

Nevertheless, the link between neuronal sensitivity to scrapie prions and cerebellar compartmentation appears to be more complex than related to the sole ZII/AldC pattern. Indeed, PC loss can be detected in the three PrP^{22L}+ bands crossing the IXth and Xth lobules of the vermis. Although most of the PCs of the IXth and Xth lobules of the vermis express ZII/AldC and EAAT4, this PrP^{22L}+ particular pattern is also reminiscent of the specific expression pattern of the heat shock protein 25 (Hsp25) in PCs (7). Interestingly, Hsp25 is only expressed by a PC subpopulation in the vermis but not in the hemispheres and its neuroprotective function could be altered along prion infection. This suggests that PrP^{22L} prion pathogenesis could be influenced by either hemisphere- or vermis-specific, unidentified zebrins.

Glial responses to 22L prions follow patterns of PC fate

Patterned microgliosis reveals ambivalent contribution of microglia to neuroprotection and neurodegeneration

Our results indicate general reactive microgliosis throughout the prion-invaded tissue. Activated microglia were observed in the whole cerebellar cortex of 22L-infected, clinically ill mice in zones where PrP^{22L} had not yet accumulated and were more dense in zones where PrP^{22L} accumulated and most PCs disappeared. The contribution of microglia to prion disease remains debated. It is classically admitted that microglia contribute to neuroinflammation and neuronal damage in neurodegenerative diseases, including prion diseases (51, 63, 81, 94, 114, 127). However, increasing evidence suggests that microglia also exerts neuroprotection (60, 96). The activation of microglia in the 22L-infected cerebellar cortex might reflect an initial protective immune response, while the more robust microglial reaction provoked by PrP^{22L} and/or neuronal death in the PrP^{22L} stripes would exacerbate neurodegeneration.

Histological and cytological compartmentation patterns of astrogliosis support a dual neuroprotective and neurodegenerative response of astrocytes along prion disease

In this study, we also reported on the gliosis of the Bergmann astrocytes that is exclusively confined to the PrP^{22L}+ stripes where massive PC loss occurs. Of note, a strong increase in GFAP-immunoreactivity surrounding PCs has been shown to precede PC loss in the cerebellar cortex of scrapie-infected sheep (80, 85) before the pathological and spongiform changes (49, 62). Although this intense glial reaction has been proposed to be associated with the removal or control of PrP^{Sc} deposits and thereby some protective role, the consistent loss of PCs in these areas also argues for an astrocytic contribution to prion pathology (28, 59, 64, 73). In prion diseases, astrocytes may lose their synapse homeostatic function

(54). Astrocytes may also exert direct neurotoxic effects by fueling the production of PrP^{Sc} and by exacerbating neuroinflammation. Astrocytes are indeed targets for prions causing human CJD and animal TSEs (78). A role of astrocytes in PrP^{Sc} production (34, 133) is further supported by the close association of the Bergmann glia with PCs (131) and Bergmann radial gliosis in ovine scrapie (53, 103) and human TSEs (31) as well as experimental rodent prion diseases (47). Interestingly, in the ML of the normal mouse, the expression pattern of ecto-5'-nucleotidase by Bergmann glia and postsynaptic PC spines corresponds to the banding pattern of ZII/AldC+ PCs (8, 110). In 22L-infected mice, the vertical palisades of PrP^{22L} deposits formed PrP^{22L}(+), PC-deprived stripes in the ML that are reminiscent of the vertical palisades of Bergmann astrocytes. At the ultrastructural level, the PrP^{22L} (or PrP^{ME7}) immunoperoxidase labeling profiles resemble that of astrocytic processes surrounding remnants of PC dendrites and synapses in the PrP^{Sc}(+) stripes. Our observations again lend support to the concept that astrocytes play a role in PrP^{Sc} production, the development and progression of the scrapie disease.

Our recent work established that upregulation of type 1 TNF- α receptor type 1 (TNFR1) at the plasma membrane of neuronal cells infected by distinct prion strains is a critical event for neurodegeneration (2, 95). The accumulation of TNFR1 at the cell surface originates from a defect of TNFR1 shedding and renders prion-infected neurons highly vulnerable to TNF- α toxicity, even if TNF- α is secreted at low doses by reactive microglia (25, 120). Here, we were unable to detect any increase in the TNFR1 level in the most vulnerable Z[−] PCs of the cerebellar cortex of 22L-infected mice, probably because of the rapid loss of these neurons in the PrP^{22L}-enriched stripes. This does not formally exclude that a transient rise of TNFR1 in PCs sensitive to prion infection provokes their death prior to PrP^{22L} accumulation.

We instead found that TNFR1 increased in Z⁺ PC stripes and followed an expression pattern complementary to that of astrocytic GFAP in the PrP^{22L}-enriched, PC-depleted stripes, suggesting that the rise of TNFR1 level does not relate to astrogliosis. TNFR1 signal is associated with the terminal processes of Bergmann astrocytes, but not PC or presynaptic parallel fiber profiles. At the ultrastructural level, TNFR1 is detected at the plasma membrane of glial processes surrounding the excitatory synapses made by parallel fibers on PC spines. This indicates that (i) cell surface TNFR1 expression in Z⁺ PCs is not enhanced by prion infection, preserving these PCs from TNF- α toxicity, and (ii) TNFR1 shedding may also be disturbed in astrocytes upon prion infection. What is thus the functional role of TNFR1 increase in prion-infected astrocytes? Of note, Bergmann glial cell processes ensheathing PCs (90) have been shown to contribute to synapse protection (55). The increase in TNFR1 level on the glial membrane facing the PC spine, that is, the postsynaptic part of these synapses, might reflect some synaptic protective response to the prion attack. Astrocyte TNFR1 expression indeed occurs exclusively close to surviving PCs, although we cannot formally rule out that the accumulation of TNFR1 at the perisynaptic astrocyte membrane leads to the degeneration of PC spines, the compartment which has been shown to be the most sensitive to 22L prions in the mouse cerebellum (115). In addition, astrogliosis in scrapie-infected brain is mediated by the JAK-STAT pathway (87), which is under the control of several receptors, including TNFR1 and other inflammatory mediators produced during gliosis in prion diseases (72).

The dual response of Bergman astrocytes to 22L prions, that is, up-regulation of GFAP in PC-deprived stripes and up-regulation of TNFR1 close to postsynaptic PC spines in resistant PC stripes suggests the following hypothetical scenario, in which TNFR1 on astrocyte envelope of PC postsynaptic spines exerts some early protective response to neuroinvasion preceding astrogliosis with up-regulated GFAP as a cause or a result of PC death.

CONCLUSION

The parasagittal compartmentation of the mouse cerebellar cortex appears to restrict 22L scrapie pathogenesis including PrP^{22L} accumulation, PC neurodegeneration and gliosis. Whereas the banding pattern of PrP^{22L} accumulation is most likely delineated by structural constraints of compartmentation, different biochemical properties of PC subpopulations might determine their differential resistance to the scrapie prions. The increase in TNFR1 levels on perisynaptic astrocytes adjacent to PC spines emerges as an early event preceding PrP^{22L} precipitation, GFAP astrogliosis and PC death, and whose contribution to prion pathogenesis remains to be investigated. Although the cell type responsible for PrP^{22L} production is still uncertain, the present data suggest a critical role of astrocytes in prion pathogenesis.

ACKNOWLEDGMENTS

The authors thank Dr. P. Isope and Pr. R. Hawkes for their helpful comments and Dr. J. Rothstein for kindly supplying the EAAT4-eGFP transgenic mice. We also thank Guy Bombarde¹ for his excellent technical assistance in immunohistochemistry, Laetitia Herzog⁵ and Fabienne Reine⁵ for their excellent technical help, Dr. S. Reibel-Foisset, N. Lethenet and M. Banni for animal breeding in the Chronobiotron (UMS3415 CNRS & Uds, Strasbourg). J.E. was supported by a grant from the Domaine d'Intérêt Majeur Cerveau Pensée of Région Ile-de-France.

REFERENCES

- Aguzzi A, Polymenidou M (2004) Mammalian prion biology: one century of evolving concepts. *Cell* **116**:313–327.
- Alleaume-Buteaux A, Nicot S, Pietri M, Baudry A, Dakowski C, Tixador P *et al* (2015) Double-edge sword of sustained ROCK activation in prion diseases through neuritogenesis defects and prion accumulation. *PLoS Pathog* **11**:e1005073. doi: 10.1371/journal.ppat.1005073.
- Apps R, Hawkes R (2009) Cerebellar cortical organization: a one-map hypothesis. *Nat Rev Neurosci* **10**:670–681. doi: 10.1038/nrn2698.
- Armstrong R, Cairns N (2003) Spatial patterns of the pathological changes in the cerebellar cortex in sporadic Creutzfeldt-Jakob disease (sCJD). *Folia Neuropathol* **41**:183–189.
- Armstrong R, Cairns N, Lantos P (2001) Spatial pattern of prion protein deposits in patients with sporadic Creutzfeldt-Jakob disease. *Neuropathology* **21**:19–24.
- Armstrong R, Ironside J, Lantos P, Cairns N (2009) A quantitative study of the pathological changes in the cerebellum in 15 cases of variant Creutzfeldt-Jakob disease (vCJD). *Neuropathol Appl Neurobiol* **35**:36–45. doi: 10.1111/j.1365-2990.2008.00979.x.
- Armstrong C, Krueger-Naug A, Currie R, Hawkes R (2000) Constitutive expression of the 25-kDa heat shock protein Hsp25 reveals novel parasagittal bands of Purkinje cells in the adult mouse cerebellar cortex. *J Comp Neurol* **416**:383–397.
- Bailly Y, Schoen SW, Delhay-Bouchaud N, Kreutzberg GW, Mariani J (1995) 5'-Nucleotidase activity as a synaptic marker of parasagittal compartmentation in the mouse cerebellum. *J Neurocytol* **24**:879–890.
- Balaban CD, Severs WB (1991) Toxic effects of somatostatin in the cerebellum and vestibular nuclei: multiple sites of action. *Neurosci Res* **12**:140–150.
- Bartz JC, Kincaid AE, Bressen RA (2002) Retrograde transport of transmissible mink encephalopathy within descending motor tracts. *J Virol* **76**:5759–5768.
- Beekes M, Mc Bride PA (2007) The spread of prions through the body in naturally acquired transmissible spongiform encephalopathies. *FEBS J* **274**:588–605.
- Berciano J, Berciano MT, Polo JM, Figols J, Ciudad J, Lafarga M (1990) Creutzfeldt-Jakob disease with severe involvement of cerebral white matter and cerebellum. *Wirschows Arch* **417**:533–538.
- Béringue V, Mallinson G, Kaisar M, Tayebi M, Sattar Z, Jackson G *et al* (2003) Regional heterogeneity of cellular prion protein isoforms in the mouse brain. *Brain* **126**:2065–2073.
- Brasko J, Rai P, Sabol MK, Patrikios P, Ross DT (1995) The AMPA antagonist NBQX provides partial protection of rat cerebellar Purkinje cells after cardiac arrest and resuscitation. *Brain Res* **699**:133–138.
- Brochu G, Maler L, Hawkes R (1990) Zebirin II: a polypeptide antigen expressed selectively by Purkinje cells reveals compartments in rats and fish cerebellum. *J Comp Neurol* **291**:538–552.
- Brown D (1999) Prion protein peptide neurotoxicity can be mediated by astrocytes. *J Neurochem* **73**:1105–1113.
- Brown P (2001) The pathogenesis of transmissible spongiform encephalopathy: routes to the brain and the erection of therapeutic barricades. *Cell Mol Life Sci* **58**:259–265.
- Brown P, Cervenakova L (2005) A prion lexicon (out of control). *Lancet* **365**:122.
- Bruce M, McBride P, Jeffrey M, Scott J (1994) PrP in pathology and pathogenesis in scrapie-infected mice. *Mol Neurobiol* **8**:105–112.
- Bruce ME, McConnell I, Fraser H, Dickinson AG (1991) The disease characteristics of different strains of scrapie in Sinc congenic mouse lines: implications for the nature of the agent and host control of pathogenesis. *J Gen Virol* **72**:595–603.
- Budka H, Aguzzi A, Brown P, Brucher JM, Bugiani O, Gullotta F *et al* (1995) Neuropathological diagnostic criteria for Creutzfeldt-Jakob disease (CJD) and other human spongiform encephalopathies (prion disease). *Brain Pathol* **5**:459–466.
- Cali I, Castellani R, Yuan J, Al-Shekhlee A, Cohen ML, Xiao X *et al* (2006) Classification of sporadic Creutzfeldt-Jakob disease revisited. *Brain* **129**:2266–2277.
- Cali I, Miller CJ, Parisi J, Geschwind M, Gambetti P, Schonberger L (2015) Distinct pathological phenotypes of Creutzfeldt-Jakob disease in recipients of prion-contaminated growth hormone. *Acta Neuropathol* **3**:37–46.
- Camoy J-B (1887) *Cellule*, 3:276.
- Carroll J, Striebel J, Race B, Phillips K, Chesebro B (2015) Prion infection of mouse brain reveals multiple new upregulated genes involved in neuroinflammation or signal transduction. *J Virol* **89**:2388–2404. doi: 10.1128/JVI.02952-14.
- Carulla P, Llorens F, Matamoros-Angles A, Aguilar-Calvo P, Espinosa JC, Gavín R *et al* (2015) Involvement of PrP(C) in kainate-induced excitotoxicity in several mouse strains. *Sci Rep* **5**:11971. doi: 10.1038/srep11971.
- Cheng X, Shen Y, Li R (2014) Targeting TNF: a therapeutic strategy for Alzheimer's disease. *Drug Discov Today* **19**:1822–1827. doi: 10.1016/j.drudis.2014.06.029.

28. Crespo I, Roomp K, Jurkowski W, Kitano H, del Sol A (2012) Gene regulatory network analysis supports inflammation as a key neurodegeneration process in prion disease. *BMC Syst Biol* **6**:132. doi: 10.1186/1752-0509-6-132.
29. Cunningham C, Deacon R, Chan K, Boche D, Rawlins J, Perry VH (2005) Neuropathologically distinct prion strains give rise to similar temporal profiles of behavioral deficits. *Neurobiol Dis* **18**:258–269.
30. DeArmond S (2001) Differential targeting of neurons by prion strains. *Methods Mol Med* **59**:85–110.
31. DeArmond S, Qiu Y, Sánchez H, Spilman P, Ninchak-Casey A, Alonso D, Daggett V (1999) PrP^C glycoform heterogeneity as a function of brain region: implications for selective targeting of neurons by prion strains. *J Neuropathol Exp Neurol* **58**:1000–1009.
32. DeArmond S, Sanchez H, Yehiely F, Qiu Y, Ninchak-Casey A, Daggett V et al (1997) Selective neuronal targeting in prion disease. *Neuron* **19**:1337–1348.
33. Dehnes Y, Chaudry FA, Ullensvang K, Lehre KP, Storm-Mathisen J, Danbolt NC (1998) The glutamate transporter EAAT4 in rat cerebellar Purkinje cells: a glutamate-gated chloride channel concentrated near the synapse in parts of the dendritic membrane facing astroglia. *J Neurosci* **18**:3606–3619.
34. Diedrich J, Bendheim P, Kim Y, Carp R, Haase A (1991) Scrapie-associated prion protein accumulates in astrocytes during scrapie infection. *Proc Natl Acad Sci USA* **88**:375–379.
35. Dusart I, Morel MP, Sotelo C (1994) Parasagittal compartmentation of adult rat Purkinje cells expressing the low-affinity nerve growth factor receptor: changes of pattern expression after traumatic lesion. *Neuroscience* **63**:351–356.
36. Edwards MA, Crandall JE, Leclerc N, Yamamoto M (1994) Effects of nervous mutation on Purkinje cell compartments defined by zebrin II and 9-O-acetylated gangliosides expression. *Neurosci Res* **19**:167–174.
37. Faucheux B, Morain E, Diouron V, Brandel J, Salomon D, Sazdovitch V et al (2011) Quantification of surviving cerebellar granule neurons and abnormal prion protein (PrP^{Sc}) deposition in sporadic Creutzfeldt-Jakob disease supports a pathogenic role for small PrP^{Sc} deposits common to the various molecular subtypes. *Neuropathol Appl Neurobiol* **37**:500–512. doi: 10.1111/j.1365-2990.2011.01179.x.
38. Fleisch VC, Leighton PL, Wang H, Pillay LM, Ritzel RG, Bhinder G et al (2013) Targeted mutation of the gene encoding prion protein in zebrafish reveals a conserved role in neuron excitability. *Neurobiol Dis* **55**:11–25. doi: 10.1016/j.nbd.2013.03.007.
39. Fletcher C, Lutz C, O'Sullivan T, Shaughnessy J, Hawkes R, Frankel W et al (1996) Absence epilepsy in tottering mutant mice is associated with calcium channel defects. *Cell* **87**:607–617.
40. Fletcher C, Tottene A, Lennon V, Wilson S, Dubel S, Paylor R et al (2001) Dystonia and cerebellar atrophy in Cacna1a null mice lacking P/Q calcium channel activity. *FASEB J* **15**:1288–1290.
41. Forloni G, Angeretti N, Chiesa R, Monzani E, Salmons M, Bugiani O, Tagliavini F (1993) Neurotoxicity of a prion protein fragment. *Nature* **362**:543–546.
42. Fraser H (1979) Neuropathology of scrapie: the precision of lesion and their diversity. In: *Slow Transmissible Diseases of the Nervous System*, pp. 387–406. SB Prusiner, WJ Hadlow eds., Academic Press: New York.
43. Fraser H (1982) Neuronal spread of scrapie agent and targeting of lesions within the retino-tectal pathway. *Nature* **295**:149–150.
44. Fraser H, Dickinson AG (1968) The sequential development of the brain lesion of scrapie in three strains of mice. *J Comp Pathol* **78**:301–311.
45. Fraser J, Halliday W, Brown D, Belichenko P, Jeffrey M (1996) Mechanisms of scrapie-induced neuronal cell death. In: *Transmissible Subacute Spongiform Encephalopathies: Prion Diseases*. Court L, Dodet B (eds), pp. 107–112. Elsevier: Paris.
46. Fujita H, Morita N, Furuichi T, Sugihara I (2012) Clustered fine compartmentalization of the mouse embryonic cerebellar cortex and its rearrangement into the postnatal striped configuration. *J Neurosci* **32**:15688–15703. doi: 10.1523/JNEUROSCI.1710-12.2012.
47. Furooka H, Horiuchi M, Yamakawa Y, Sata T (2011) Predominant involvement of the cerebellum in guinea pigs infected with bovine spongiform encephalopathy (BSE). *J Comp Pathol* **144**:269–276. doi: 10.1016/j.jcpa.2010.10.004.
48. Gabe M (1968) *Techniques Histologiques*, pp. 225–227. Masson & Cie Eds: Paris.
49. Georgsson G, Gisladdottir E, Arnadottir S (1993) Quantitative assessment of the astrocytic response in natural scrapie of sheep. *J Comp Pathol* **108**:229–240.
50. Ghetti B, Piccardo P, Frangione B, Bugiani O, Giaccone G, Young K et al (1996) Prion protein amyloidosis. *Brain Pathol* **6**:127–145.
51. Giese A, Brown D, Groschup M, Feldmann C, Haist I, Kretzschmar H (1998) Role of microglia in neuronal cell death in prion disease. *Brain Pathol* **8**:449–457.
52. Gincel D, Regan M, Jin L, Watkins A, Bergles DE, Rothstein J (2006) Analysis of cerebellar Purkinje cells using EAAT4 glutamate transporter promoter reporter in mice generated via bacterial artificial chromosome-mediated transgenesis. *Exp Neurol* **203**:205–212.
53. Gonzales L, Martin S, Jeffrey M (2003) Distinct profiles of PrP(d) immunoreactivity in the brain of scrapie- and BSE-infected sheep: implications for differential cell targeting and PrP processing. *J Gen Virol* **84**:1339–1350.
54. Graeber M (2010) Changing face of microglia. *Science* **330**:783–788. doi: 10.1126/science.1190929.
55. Grosche J, Matyash V, Möller T, Verkhratsky A, Reichenbach A, Kettenmann H (1999) Microdomains for neuron-glia interaction: parallel fiber signaling to Bergmann glial cells. *Nat Neurosci* **2**:139–143.
56. Guentchev M, Wanschitz J, Voigtlander T, Flicker H, Budka H (1999) Selective neuronal vulnerability in human prion disease – fatal familial insomnia differs from other types of prion diseases. *Am J Pathol* **155**:1453–1457.
57. Haw JJ, Gray F, Baudrimont M, Escourolle R (1981) Cerebellar changes in 50 cases of Creutzfeldt-Jakob disease with emphasis on granule cell atrophy variant. *Acta Neuropathol (Berl)* **7**:196–198.
58. Hawkes R (2014) Purkinje cell stripes and long-term depression at the parallel fiber-Purkinje cell synapse. *Front Syst Neurosci* **8**:41. doi: 10.3389/fnsys.2014.00041.
59. Hernandez R, Sarasa R, Toledano A, Badiola J, Monzon M (2014) Morphological approach to assess the involvement of astrocytes in prion propagation. *Cell Tissue Res* **358**:57–63. doi: 10.1007/s00441-014-1928-3.
60. Hines DJ, Hines RM, Mulligan SJ, Macvicar BA (2009) Microglia processes block the spread of damage in the brain and require functional chloride channels. *Glia* **57**:1610–1618. doi: 10.1002/glia.20874.
61. Jarius C, Kovacs GG, Belay G, Hainfellner JA, Mitrova E, Budka H (2003) Distinctive cerebellar immunoreactivity for the prion protein in familial (E200K) Creutzfeldt-Jakob disease. *Acta Neuropathol* **105**:449–454.
62. Jeffrey M, González L (2007) Classical sheep transmissible spongiform encephalopathies: pathogenesis, pathological phenotypes and clinical disease. *Neuropathol Appl Neurobiol* **33**:373–394.
63. Jeffrey M, Halliday W, Bell J, Johnston A, MacLeod N, Ingham C et al (2000) Synapse loss associated with abnormal PrP precedes neuronal degeneration in the scrapie-infected murine hippocampus. *Neuropathol Appl Neurobiol* **26**:41–54.
64. Jeffrey M, Martin S, Barr J, Chong A, Fraser JR (2001) Onset of accumulation of PrPres in murine ME7 scrapie in relation to pathological and PrP immunohistochemical changes. *J Comp Pathol* **124**:20–28.

65. Jeffrey M, Mc Govern G, Sisó S, González L (2011) Cellular and subcellular pathology of animal prion diseases: relationship between morphological changes, accumulation of abnormal prion protein and clinical disease. *Acta Neuropathol* **121**:113–134. doi: 10.1007/s00401-010-0700-3.
66. Karapetyan Y, Saa P, Mahal S, Sferrazza GF, Sherman A, Sales N et al (2009) Prion strain discrimination based on rapid in vivo amplification and analysis by the cell panel assay. *PLoS One* **4**:e5730. doi: 10.1371/journal.pone.0005730.
67. Kim YS, Carp RI, Callahan SM, Natelli M, Wisniewski HM (1990) Vacuolization, incubation period and survival time analyses in three brain regions with the 22L scrapie strain. *J Neuropathol Exp Neurol* **49**:106–113.
68. Kim YS, Carp RI, Callahan SM, Wisniewski HM (1987) Incubation periods and survival times for mice injected stereotactically with three scrapie strains in different brain regions. *J Gen Virol* **68**:685–702.
69. Kimberlin R, Walker C, Fraser H (1989) The genomic identity of different strains of mouse scrapie is expressed in hamsters and preserved on reisolation in mice. *J Gen Virol* **70**:2017–2025.
70. King A, Doey L, Rossor M, Mead S, Collinge J, Lantos P (2003) Phenotypic variability in the brains of a family with a prion disease characterized by a 144-base pair insertion in the prion protein gene. *Neuropathol Appl Neurobiol* **29**:98–105.
71. Kitamoto T, Shin RW, Doh-ura K, Tomokane N, Miyazono M, Muramoto T, Tateishi J (1992) Abnormal isoform of prion proteins accumulates in the synaptic structures of the central nervous system in patients with Creutzfeldt-Jakob disease. *Am J Pathol* **140**:1285–1294.
72. Kiu H, Nicholson S (2012) Biology and significance of the JAK/STAT signaling pathways. *Growth Factors* **30**:88–106. doi: 10.3109/08977194.2012.660936.
73. Krasemann S, Neumann M, Luepke J, Grashorn J, Wurr S, Stocking C, Glatzel M (2012) Persistent retroviral infection with MoMuLV influences neuropathological signature and phenotype of prion disease. *Acta Neuropathol* **124**:111–126. doi: 10.1007/s00401-012-0944-1.
74. Kretschmar HA, Kitamoto T, Doerschott J, Mehraein P, Tateishi J (1991) Diffuse deposition of immunohistochemically labeled prion protein in the granular layer of the cerebellum in a patient with Creutzfeldt-Jakob disease. *Acta Neuropathol* **82**:536–540.
75. Langeron M (1942) *Précis de Microscopie*, p. 394. Masson & Cie: Paris.
76. Lasmezas CI, Deslys JP, Demaimay R, Adjou KT, Haw JJ, Dormont D (1996) Strain specific and common pathogenic events in murine models of scrapie and bovine spongiform encephalopathy. *J Gen Virol* **77**:1601–1609.
77. Lawson VA, Collins SJ, Masters CL, Hill AF (2005) Prion protein glycosylation (review). *J Neurochem* **39**:793–801.
78. Lefrançois T, Fages C, Brugere-Picoux J, Tardy M (1994) Astroglial reactivity in natural scrapie of sheep. *Microb Pathog* **17**:283–289.
79. Lucassen PJ, Williams A, Chung WCJ, Fraser H (1995) Detection of apoptosis in murine scrapie. *Neurosci Lett* **198**:185–188.
80. Manuelidis L, Tesin D, Sklaviadis T, Manuelidis E (1987) Astrocyte gene expression in Creutzfeldt-Jakob disease. *Proc Natl Acad Sci USA* **84**:5937–5941.
81. Marella M, Chabry J (2004) Neurons and astrocytes respond to prion infection by inducing microglia recruitment. *J Neurosci* **24**:620–627.
82. Marzban H, Sillitoe R, Hoy M, Chung S, Rafuse V, Hawkes R (2004) Abnormal HNK-1 expression of an N-CAM null mouse. *J Neurocytol* **33**:117–130.
83. Mateos JM, Osorio A, Azkue JJ, Benitez R, Elezgarri I, Bilbao A et al (2001) Parasagittal compartmentalization of the metabotropic glutamate receptor mGluR1b in the cerebellar cortex. *Eur J Anat* **5**:15–21.
84. Mitrova E, Mayer V, Orolin D (1978) Transmissible virus dementia. II. Neurohistology of three, geographically clustered cases of Creutzfeldt-Jakob disease. *Acta Virol* **22**:154–161.
85. Moser M, Colello R, Pott U, Oesch B (1995) Developmental expression of the prion protein gene in glial cells. *Neuron* **14**:509–517.
86. Müller W, Ushijima H, Schröder H, Forrest J, Schatton W, Rytik P, Heffner-Laue M (1993) Cytoprotective effect of NMDA receptor antagonists on prion protein (Prion^{Sc})-induced toxicity in rat cortical cell cultures. *Eur J Pharmacol* **246**:261–267.
87. Na Y, Jin J, Kim J, Choi E, Carp R, Kim Y (2007) JAK-STAT signaling pathway mediates astrogliosis in brains of scrapie-infected mice. *J Neurochem* **103**:637–649.
88. Novitskaya V, Bocharova O, Bronstein I, Baskakov I (2006) Amyloid fibrils of mammalian prion protein are highly toxic to cultured cells and primary neurons. *J Biol Chem* **281**:13828–13836.
89. O'Hearn E, Molliver M (1993) Degeneration of Purkinje cells in parasagittal zones of the cerebellar vermis after treatment with ibogaine or harmaline. *Neuroscience* **55**:303–310.
90. Palay S, Chan-Palay V (1974) *Cerebellar Cortex. Cytology and Organization*. Springer: New York.
91. Parchi P, Giese A, Capellari S, Brown P, Schulz-Schaeffer W, Wind O et al (1999) Classification of sporadic Creutzfeldt-Jakob disease based on molecular and phenotypic analysis of 300 subjects. *Ann Neurol* **46**:224–233.
92. Parchi P, Strammiello R, Giese A, Kretschmar H (2011) Phenotypic variability of sporadic human prion disease and its molecular basis: past, present and future. *Acta Neuropathol* **121**:91–112. doi: 10.1007/s00401-010-0779-6.
93. Paxinos G, Franklin K (2001) *The Mouse Brain in Stereotaxic Coordinates*. Acad Press, London, UK.
94. Perry VH, Nicoll JA, Holmes C (2010) Microglia in neurodegenerative disease. *Nat Rev Neurol* **6**:193–201. doi: 10.1038/nrneuro.2010.17.
95. Piétri M, Dakowski C, Hannaoui S, Alleaume-Buteaux A, Hernandez-Rapp J, Ragagnin A et al (2013) PDK1 decreases TACE-mediated α -secretase activity and promotes disease progression in prion and Alzheimer's diseases. *Nat Med* **19**:1124–1131. doi: 10.1038/nm.3302.
96. Power JH, Blumbergs PC (2009) Cellular glutathione peroxidase in human brain: cellular distribution, and its potential role in the degradation of Lewy bodies in Parkinson's disease and dementia with Lewy bodies. *Acta Neuropathol* **117**:63–73. doi: 10.1007/s00401-008-0438-3.
97. Prusiner S (1982) Novel proteinaceous infection particles cause scrapie. *Science* **216**:136–144.
98. Prusiner S (1997) Prion diseases and the BSE crisis. *Science* **278**:245–251.
99. Quinn M, Kim Y, Lossinsky A, Carp R (1988) Influence of stereotactically injected scrapie on neurotransmitter systems of mouse cerebellum. *Brain Res* **445**:297–302.
100. Reeber SL, Otis TS, Sillitoe RV (2013a) New roles for the cerebellum in health and disease. *Front Syst Neurosci* **7**:1–11. doi: 10.3389/fnsys.2013.00083.
101. Reeber SL, White JJ, Georges-Jones NA, Sillitoe RV (2013b) Architecture and development of olivo-cerebellar circuit topography. *Front Neural Circuits* **6**:115. doi: 10.3389/fncir.2012.00115.
102. Sandberg M, Al-Doujaily H, Sharps B, Clarke A, Collinge J (2011) Prion propagation and toxicity *in vivo* occur in two distinct mechanistic phases. *Nature* **470**:540–542. doi: 10.1038/nature09768.
103. Sarasa R, Martinez A, Monleon E, Bolea R, Vargas A, Badiola J, Monzon M (2012) Involvement of astrocytes in transmissible spongiform encephalopathies: a confocal microscope study. *Cell Tissue Res* **350**:127–134. doi: 10.1007/s00441-012-1461-1.

104. Sarna JR, Hawkes R (2003) Patterned Purkinje cell death in the cerebellum. *Prog Neurobiol* **70**:473–507.
105. Sarna JR, Larouche M, Marzban H, Sillitoe R, Rancourt D, Hawkes R (2003) Patterned Purkinje cell degeneration in mouse models of Niemann-Pick type C disease. *J Comp Neurol* **456**:279–291.
106. Sarna JR, Miranda S, Schuchman E, Hawkes R (2001) Patterned cerebellar Purkinje cell death in a transgenic mouse model of Niemann-Pick type A/B disease. *Eur J Neurosci* **13**:1873–1880.
107. Scalzo P, Kümmer A, Cardoso F, Teixeira A (2009) Increased serum levels of soluble tumor necrosis factor- α -receptor-1 in patients with Parkinson's disease. *J Neuroimmunol* **216**:122–125. doi: 10.1016/j.jneuroim.2009.08.001.
108. Schorge S, van de Leemput J, Singleton A, Houlden H, Hardy J (2010) Human ataxias: a genetic dissection of inositol triphosphate receptor (ITPR1)-dependent signaling. *Trends Neurosci* **33**:211–219. doi: 10.1016/j.tins.2010.02.005.
109. Schulz-Schaeffer WJ, Giese A, Windl O, Kretschmar HA (1996) Polymorphism at codon 129 of the prion protein gene determines cerebellar pathology in Creutzfeldt-Jakob disease. *Clin Neuropathol* **15**:353–357.
110. Scott T (1963) A unique pattern of localization within the cerebellum. *Nature* **200**:793.
111. Scott JR, Fraser H (1989) The 2nd nerve and its central projections as a simple scrapie model. In: *Unconventional Virus Diseases of the Central Nervous System*. Court LA, Dormont D, Brown P, Kingsbury DT (eds), pp. 573–586. Commissariat à l'Energie Atomique, Fontenay-aux-Roses: France.
112. Selimi F, Doughty M, Delhay-Bouchaud N, Mariani J (2000) Target-related and intrinsic neuronal death in Lurcher mutant mice are both mediated by caspase-3 activation. *J Neurosci* **20**:992–1000.
113. Selimi F, Lohof AM, Heitz S, Lalouette A, Jarvis CI, Bailly Y, Mariani J (2003) Lurcher GRID2-induced death and depolarization can be dissociated in cerebellar Purkinje cells. *Neuron* **37**:813–819.
114. Shi F, Yang L, Kouadir M, Yang Y, Wang J, Zhou X et al (2012) The NALP3 inflammasome is involved in neurotoxic prion peptide-induced microglial activation. *J Neuroinflammation* **9**:73. doi: 10.1186/1742-2094-9-73.
115. Siskova Z (2013) How structure shapes (dys)function. A perspective to understanding brain-region-specific degeneration in prion disease. *Prion* **7**:291–293. doi: 10.4161/pri.26019.
116. Siskova Z, Reynolds R, O'Connor V, Perry V (2013) Brain region specific pre-synaptic and post-synaptic degeneration are early components of neuropathology in prion disease. *PLoS One* **8**:e55004. doi: 10.1371/journal.pone.0055004.
117. Somerville R (2013) How independent are TSE agents from their hosts? *Prion* **7**:272–275. doi: 10.4161/pri.25420.
118. Telling G (2013) The importance of prions. *PLoS Pathog* **9**:e1003090. doi: 10.1371/journal.ppat.1003090.
119. Tolbert DL, Bradley MW, Tolod EG, Torres-Aleman I, Clark BR (2001) Chronic intraventricular infusion of glial cell line-derived neurotrophic factor (GDNF) rescues some cerebellar Purkinje cells from heterodegeneration. *Exp Neurol* **170**:375–379.
120. Tribouillard-Tanvier D, Striebel J, Peterson K, Chesebro B (2009) Analysis of protein levels of 24 cytokines in scrapie agent-infected brain and glial cell cultures from mice differing in prion protein expression levels. *J Virol* **83**:11244–11253. doi: 10.1128/JVI.01413-09.
121. Vidal C, Herzog C, Haeberle A-M, Bombarde G, Miquel M-C, Carimalo J et al (2009) Early dysfunction of central 5-HT system in a murine model of bovine spongiform encephalopathy. *Neuroscience* **160**:731–743. doi: 10.1016/j.neuroscience.2009.02.072.
122. Vilette D, Andreoletti O, Archer F, Madelaine MF, Vilotte JL, Lehmann S, Laude H (2001) *Ex vivo* propagation of infectious sheep scrapie agent in heterologous epithelial cells expressing ovine prion protein. *Proc Natl Acad Sci USA* **98**:4055–4059.
123. Vital C, Gray F, Vital A, Parchi P, Capellari S, Petersen RB et al (1998) Prion encephalopathy with insertion of octapeptide repeats: the number of repeats determines the type of cerebellar deposits. *Neuropathol Appl Neurobiol* **24**:125–130.
124. Wang WY, Tan MS, Yu JT, Tan L (2015) Role of pro-inflammatory cytokines released from microglia in Alzheimer's disease. *Ann Transl Med* **3**:136. doi:10.3978/j.issn.2305-5839.2015.03.49.
125. Welsh JP, Yuen G, Placantonakis DG, Vu TQ, Haiss F, O'Hearn E et al (2002) Why do Purkinje cells die so easily after global brain ischemia? Aldolase C, EAAT4, and the cerebellar contribution to posthypoxic myoclonus. *Adv Neurol* **89**:331–359.
126. Wemheuer WM, Benestad S, Wrede A, Wemheuer WE, Brenig B, Bratberg B, Schulz-Schaeffer W (2011) PrP spreading patterns in the brain of sheep linked to different prion types. *Vet Res* **42**:32. doi: 10.1186/1297-9716-42-32.
127. Williams A, Lawson L, Perry V, Fraser H (1994) Characterization of the microglial response in scrapie. *Neuropathol Appl Neurobiol* **20**:47–55.
128. Williams A, van Dam A-M, Eikelenboom P, Fraser H (1997) Immunocytochemical appearance of cytokines, prostaglandin E2 and lipocortin-1 in the CNS during the incubation period of murine scrapie correlates with progressive PrP accumulations. *Brain Res* **754**:171–180.
129. Williams A, Lucassen P, Ritchie D, Bruce M (1997) PrP deposition, microglial activation and neuronal apoptosis in murine scrapie. *Exp Neurol* **144**:433–438.
130. Xiao X, Yuan J, Haik S, Cali I, Zhan Y, Moudjou M et al (2013) Glycoform-selective prion formation in sporadic and familial forms of prion disease. *PLoS One* **8**:e58786. doi: 10.1371/journal.pone.0058786.
131. Yamada K, Watanabe M (2002) Cyto differentiation of Bergmann glia and its relationship with Purkinje cells. *Anat Sci Int* **77**:94–108.
132. Yang Q, Hashizume Y, Yoshida M, Wang Y (1999) Neuropathological study of cerebellar degeneration in prion disease. *Neuropathology* **19**:33–39.
133. Ye X, Scallet A, Kascsak R, Carp R (1998) Astrocytosis and amyloid deposition in scrapie-infected hamsters. *Brain Res* **809**:277–287.
134. Zhou H, Lin Z, Voges K, Ju C, Gao Z, Bosman LW et al (2014) Cerebellar modules operate at different frequencies. *Elife* **3**:e02536. doi: 10.7554/eLife.02536.